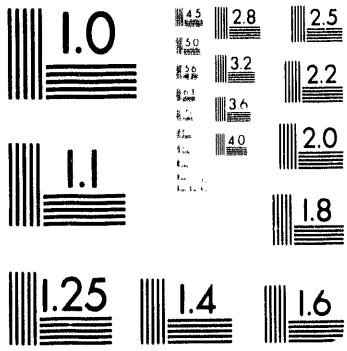
1.0
1.1
1.25
1.4
1.6
1.8
2.0
2.2
2.5
2.8
3.2
3.6
4.0
4.5
5.0

1 of 1

NODAL APPROXIMATIONS OF VARYING ORDER BY ENERGY GROUP FOR SOLVING THE DIFFUSION EQUATION

by

JILL TERESE BRODA

B.S. Nuclear Eng., Purdue University
(1990)

SUBMITTED TO THE DEPARTMENT OF
NUCLEAR ENGINEERING
IN PARTIAL FULFILLMENT OF THE REQUIREMENTS
FOR THE DEGREE OF

MASTER OF SCIENCE
IN NUCLEAR ENGINEERING

at the

MASSACHUSETTS INSTITUTE OF TECHNOLOGY
February, 1992

Signature of the Author Jill Terese Broda
Department of Nuclear Engineering
January, 1992

Certified by
Allan F. Henry
Thesis Supervisor

Accepted by
Allan F. Henry
Departmental Graduate Committee Chairman
Department of Nuclear Engineering

NODAL APPROXIMATIONS OF VARYING ORDER BY ENERGY GROUP FOR SOLVING THE DIFFUSION EQUATION

by

JILL TERESE BRODA

Submitted to the Department of Nuclear Engineering
on January 17, 1991 in partial fulfillment of the
requirements for the Degree of Master of Science in
Nuclear Engineering

ABSTRACT

The neutron flux across the nuclear reactor core is of interest to reactor designers and others. The diffusion equation, an integro-differential equation in space and energy, is commonly used to determine the flux level. However, the solution of a simplified version of this equation (multigroup form) when automated is very time consuming. Since the flux level changes with time, in general, this calculation must be made repeatedly. Therefore solution techniques that speed the calculation while maintaining accuracy are desirable.

One factor that contributes to the solution time is the spatial flux shape approximation used. It is common practice to use the same order flux shape approximation in each energy group even though this method may not be the most efficient.

The one-dimensional, two-energy group diffusion equation was solved, for the node average flux and core k-effective, using two sets of spatial shape approximations for each of three reactor types. A fourth-order approximation in both energy groups forms the first set of approximations used. The second set used combines a second-order approximation in energy group one (the fast neutron group) with a fourth-order approximation in energy group two (the slow neutron group).

Comparison of the results from the two approximation sets show that the use of a different order spatial flux shape approximation results in considerable loss in accuracy for the pressurized water reactor modeled. However, the loss in accuracy is small for the heavy water and graphite reactors modeled.

The use of different order approximations in each energy group produces mixed results. Further investigation into the accuracy and computing time is required before any quantitative advantage of the use of the second-order approximation in energy group one and the fourth-order approximation in energy group two can be determined.

Thesis Supervisor: Allan F. Henry

Title: Professor of Nuclear Engineering

Acknowledgements

There are a few people that I would like to thank for their help and support. Without them this thesis would not have been possible.

First, I would like to thank Professor Allan F. Henry, my thesis supervisor, for his guidance.

I would also like to thank my thesis reader Professor David D. Lanning for his comments and suggestions.

The Nuclear Engineering and Health Physics Fellowship program administered by Oak Ridge Associated Universities for the U.S. Department of Energy must be acknowledged. My graduate education was made possible by the financial support of this program.

Finally, I would like to thank John J. Fisher Jr. for his love and encouragement. Without his support I would not have made it through graduate school.

TABLE OF CONTENTS

	Page
Abstract	2
Acknowledgements	3
Table of Contents	4
List of Figures	6
List Tables	8
Chapter 1. Introduction	9
1.1 Motivation and Introduction	9
1.2 Background	10
1.2.1 Diffusion Theory	10
1.2.2 Nodal Methods	11
1.3 Objective and Summary	11
Chapter 2. Derivation of Nodal Equations	13
2.1 Introduction	13
2.2 Derivation of Quartic Flux Expansion	14
2.3 Derivation of the Nodal Equations for Inner Nodes	16
2.3.1 Derivation of the Flux Nodal Equation	16
2.3.2 Derivation of Third- and Fourth-Order Expansion Coefficient Nodal Equations	20
2.4 Boundary Conditions and Derivation of the Nodal Equations for Outer Nodes	22
2.4.1 Boundary Conditions	22
2.4.2 Derivation of the Flux Nodal Equation for Node N	22
2.4.3 Derivation of the Flux Nodal Equation for Node 1	23
2.4.4 Derivation of the Expansion Coefficient Nodal Equations in Node N	25
2.4.5 Derivation of the Expansion Coefficient Nodal Equations for Node 1	25
2.5 Summary	26
Chapter 3. Solution Method	27
3.1 Introduction	27
3.2 Matrix Relations	27
3.3 Solution Scheme	28
3.3.1 Flux Iteration	28
3.3.2 Quartic Expansion Coefficient Iteration	29
3.3.3 Iteration Summary	30
3.4 Summary	30

TABLE OF CONTENTS continued

	Page
Chapter 4. Application of Solution Method	32
4.1 Introduction	32
4.2 Computer Programs	32
4.3 Benchmark Problem	34
4.4 Test Problems	35
4.4.1 Graphite Reactor	35
4.4.2 Pressurized Light Water Reactor	39
4.4.3 Heavy Water Reactor	61
4.5 Summary	69
Chapter 5. Conclusions and Recommendations	70
5.1 Conclusions	70
5.2 Recommendations	70
References	72

LIST OF FIGURES

Figure	Title	Page
3.1	Schematic of iteration loops.	31
4.1	Computer program flowchart.	33
4.2	MHTGR model. Region 1 is 82.6 cm wide, region 2 is 92.1 cm wide, region 3 is 33.8 cm wide, region 4 is 33.5 cm wide, and region 5 is 54.9 cm wide. Symmetry boundary conditions on the right.	35
4.3	Energy Group One Flux as a Function of Position for the MHTGR, Energy Group Two Flux as a Function of Position for the MHTGR	38
4.4	Salem - 1 models. A and B: all regions are 21.6 cm wide except the first region which is 10.8 cm wide, symmetry boundary conditions on the left, regions 7, 8, and 9 are reflectors. C: all regions are 20 cm wide, symmetry boundary conditions on the left. D: all regions are 20 cm wide.	40
4.5	Energy Group One Flux as a Function of Position for Salem - 1 Model A, Energy Group Two Flux as a Function of Position for Salem - 1 Model A	47
4.6	Energy Group One Flux as a Function of Position for Salem - 1 Model B, Energy Group Two FLux as a Function of Position for Salem - 1 Model B	50
4.7	Energy Group One Flux as a Function of Position for Salem - 1 Model C, Energy Group Two Flux as a Function of Position for Salem - 1 Model C	52
4.8	Energy Group One Flux as a Function of Position for Salem - 1 Model D, Energy Group Two Flux as a Function of Position for Salem - 1 Model D	54
4.9	IAEA reactor model. All regions are 20 cm wide except the first region which is 10 cm wide. Symmetry boundary conditions on the left. Region 4 is a reflector.	56
4.10	Energy Group One Flux as a Function of Position for the IAEA Benchmark, Energy Group Two Flux as a Function of Position for the IAEA Benchmark	60
4.11	Production reactor slices modeled. All regions are 18 cm wide. A is symmetry boundary conditions on the right.	62

LIST OF FIGURES continued

Figure	Title	Page
4.12	Energy Group One Flux as a Function of Position for the Production Reactor Simulation Model A, Energy Group Two Flux as a Function of Position for the Production Reactor Simulation Model A	65
4.13	Energy Group One Flux as a Function of Position for the Production Reactor Simulation Model B, Energy Group Two Flux as a Function of Position for the Production Reactor Simulation Model B	67

LIST OF TABLES

Table	Title	Page
2.1	Value of polynomials when evaluated at node edges and when integrated over the node width. Adapted from reference number 4.	16
4.1	Macroscopic cross sections for graphite reactor.	36
4.2	Comparison of the node-average flux value for each node for the MHTGR. The values from Fourfour.f are larger by the percentage given.	37
4.3	Macroscopic cross sections for Salem - 1.	41
4.4	Comparison of the node-average flux value for each node of Salem - 1. The value from Fourfour.f is larger by the percentage given.	42
4.5	Comparison of the node-average flux value from a fourth-order approximation in both energy groups and a second-order approximation in both energy groups for each node of Salem - 1 model A. The value from the fourth-order approximation is larger by the percentage given.	46
4.6	Comparison of the node-average flux value from a fourth-order approximation in both energy groups and a second-order approximation in both energy groups for each node of Salem - 1 model B. The value from the fourth-order approximation is larger by the percentage given.	49
4.7	Macroscopic cross sections for IAEA Benchmark.	56
4.8	Comparison of the node-average flux value for each node of the IAEA Benchmark. The value from Fourfour.f is larger by the percentage given.	57
4.9	Comparison of the node-average flux value from a fourth-order approximation in both energy groups and a second-order approximation in both energy groups for each node of the IAEA Benchmark. The value from the fourth-order approximation is larger by the percentage given.	59
4.10	Macroscopic cross sections for production reactor.	62
4.11	Comparison of the node-average flux value for each node of the production reactor simulation. The values from Fourfour.f are larger by the percentage given.	63

Chapter 1

INTRODUCTION

1.1 Motivation and Introduction

Many characteristics of a nuclear reactor core, criticality and burnup for example, can only be determined once the neutron population in space and energy across the core is known. Calculation of the neutron population, however, is both difficult and time consuming even when automated. Therefore, methods to speed the calculation while maintaining accuracy are always being investigated.

Knowledge of the neutron population during both transient and steady-state operations is necessary. The behavior of the population during transient operation is more difficult to calculate. However, knowledge of this behavior is equally important as the knowledge of the population during steady-state conditions.

One common method for determining the neutron population for a steady-state reactor is to use the diffusion equation, an integro-differential equation in space and energy. It is standard practice when solving this equation to cast this equation into a set of space-dependent equations by partitioning the energy range into a number of "energy groups" and defining group-averaged parameters within each energy group. The result, called the few-group diffusion equations, is a set of coupled differential equations.

When solving the few-group diffusion equations, it is common practice to use a finite-difference method. However, a large number of grid points need to be used when investigating a commercial reactor core and, consequently, the computation time is considerable.

A solution technique that is becoming more common is the use of nodal methods. In this method large homogenized regions replace a number of small regions with varied compositions. The associated reduction in computation time is substantial. However, there is still room for improvement.

In addition to the number of spatial regions used in the solution method, the spatial shape of the neutron population in each region and energy group is important. The mathematical order of the assumed spatial shape of the population is directly related to the solution time and the accuracy of the solution. For each energy group, the same order/form of the spatial shape of the population is used when solving the few-group diffusion equations using nodal methods. However, the actual neutron population shape in each energy group is different. The shape in the high energy groups is much smoother than the shape in low energy groups.

The use of different order polynomials for the spatial shape of the flux, defined as the neutron density times the neutron speed, in each energy group is investigated in this thesis. The results obtained by solving the few-group diffusion equations using nodal methods with different order and the same order polynomials, by energy group, are compared. A simplified case involving only two-energy groups and a one-dimensional reactor is considered.

1.2 Background

1.2.1 Diffusion Theory

The continuous-energy diffusion equation can be derived using the P-1 approximation to the Boltzmann transport equation assuming that the source of neutrons is isotropic[11]. This assumption, however, limits the regions of the reactor in which diffusion theory can be applied. Two regions in which the theory is not valid are near boundaries and in highly absorbing materials. By integrating the continuous-energy equation over an energy group g, the few-group diffusion equations can be formed. The resulting coupled differential equations, coupled by energy groups, incorporate energy group parameters. It is through the careful definition of these parameters that the limitations on diffusion theory can be reduced.

If the reactor is partitioned into subregions and equivalent group parameters are defined such that interaction rates within each subregion are reproduced in an integral sense[2] the applicability of diffusion theory can be extended. Nodal methods can then be used to solve the few-group diffusion equations if equivalent parameters can be found such that the reactor is represented by a few large homogenized regions[3].

1.2.2 Nodal Methods

The quantities determined using nodal equations are the volume-averaged group-fluxes in each node. These fluxes are related to each other mathematically through the use of "coupling constants"[2].

An important, and difficult, step in the derivation of the nodal equations is the determination of these "coupling constants"[2]. The relation between the net current across the node surface, the node-average flux, and the node-average flux of the neighboring nodes for each energy group is governed by these constants. One way to determine the constants is to expand the transverse integrated group-fluxes in each node in polynomials. The accuracy of the "coupling constants" is then dependent on the order of the polynomials.

1.3 Objective and Summary

A comparison of the results, flux and multiplication factor, obtained by solving the two-group diffusion equation using nodal methods for equal and varied polynomial orders of the spatial shape of the flux in the two energy groups is carried out. Because of the relative simplicity of the equations to be solved, a one-dimensional reactor is used for the comparisons. The objective of this work is to determine the error introduced by using polynomials of different orders in the two energy groups. Three reactor types (pressurized

water reactor, heavy water reactor, and graphite reactor) are examined in order to gain insight into the applicability of this technique to various designs.

There are three parts to the work performed: the derivation of the nodal equations, the development of the solution technique, and the application of the solution method. Chapters 2, 3, and 4, respectively, are devoted to the discussion of each of these components. An overall summary and recommendations for further research are contained in Chapter 5.

Chapter 2

DERIVATION OF NODAL EQUATIONS

2.1 Introduction

The derivation of the nodal equations is presented in this chapter. These equations are derived for a one-dimensional system with two energy groups. Up-scatter from thermal energies and fission neutron appearance in group two are assumed to be negligible in the derivation. All of the equations are derived using a quartic approximation for the spatial shape of the flux. In this way the equations for the two energy groups can be derived simultaneously and the quadratic approximation can be obtained by simplifying the resultant equations. Because a fourth-order approximation is used, five coefficients are needed for the flux expansion in each node. Two of these coefficients can be eliminated by imposing flux and current continuity conditions at the node interfaces. Three nodal equations are needed to determine the remaining three coefficients: the node average-flux, the third-order coefficient in the flux expansion and the fourth-order coefficient in the flux expansion.

The derivation of the nodal equations begins with the determination of an equation for the scalar flux density. This is done by integrating the Boltzmann transport equation over all directions and then over energy group g and by imposing Fick's Law. The equation that results is called the multigroup diffusion equation.

In order to form the nodal equations for the node-average flux, the one-dimensional multigroup diffusion equation is integrated over the width of each node. The expression that results, called the nodal balance equation, relates the net current density at the node surfaces to the node average-flux. Fick's Law and the flux expansion are then used to form a second relation between the current density and the average flux in adjacent nodes. This second relation closes the system of equations for the flux.

The multigroup equation combined with the flux expansion is the starting point in the derivation of the nodal equations for the expansion coefficients. This equation is integrated using weighting functions to obtain a relation between the expansion constants, the current densities at the node surfaces and the node fluxes. The second relation between these parameters is obtained by combining Fick's Law and the flux expansion. Through the manipulation of the two relations found, the final form of the nodal equations for the third- and fourth-order expansion coefficients can be obtained.

2.2 Derivation of Quartic Flux Expansion

The spatial shape of the flux is assumed to be a fourth-order polynomial in the following general derivation of the nodal equations. It is convenient to assume a general form having some of the unknowns of the problem as coefficients. Accordingly the form chosen is

$$\Phi_g(x) = P_{\bar{\Phi}}(x)\bar{\Phi}_g^i + P_{\Phi^-}(x)\Phi_g^i + P_{\Phi^+}(x)\Phi_g^{i+1} + P_3(x)C_{3g}^i + P_4(x)C_{4g}^i \qquad 2.1$$

where

$P_{\bar{\Phi}}(x)$, $P_{\Phi^-}(x)$, $P_{\Phi^+}(x)$ - second order polynomials in x,

$P_3(x)$ - third order polynomial in x,

$P_4(x)$ - fourth order polynomial in x,

$\bar{\Phi}_g^i$ - average group g flux in node i,

Φ_g^i - group g flux at left edge of node i,

Φ_g^{i+1} - group g flux at right edge of node i,

C_{3g}^i - third-order expansion coefficient for group g flux in node i,

and

C_{4g}^i - fourth-order expansion coefficient for group g flux in node i.

Before Eqn. 2.1 can be used, the x-dependence of the five polynomials must be determined. This is done by placing conditions on each of the polynomials.based on the fact that the flux must equal Φ_g^i for x on the left edge of node i, equal Φ_g^{i+1} for x on the right edge of node i, and equal $\overline{\Phi}_g^i$ when integrated over the node width. Table 2.1 gives the conditions as they apply to each polynomial[4]. By applying these conditions to the polynomials of second order the resulting equations[4] are

$$P_{\Phi^-}(x) = \frac{x_{i+1} - x}{h_i}\left(1 - \frac{3}{h_i}(x - x_i)\right) = (1-v)\,(1-3v), \qquad 2.2a$$

$$P_{\Phi^+}(x) = \frac{x - x_i}{h_i}\left(1 - \frac{3}{h_i}(x_{i+1} - x)\right) = v(3v-2), \qquad 2.2b$$

and

$$P_{\overline{\Phi}}(x) = \frac{6}{h_i^2}(x - x_i)(x_{i+1} - x) = 6v(1-v) \qquad 2.2c$$

where

x_{i+1} - right edge of node i,

x_i - left edge of node i,

$h_i = x_{i+1} - x_i$, width of node i,

and

$v = (x - x_i) / h_i$.

An additional condition placed on the fourth-order polynomial is that the polynomial must be symmetric about the center of the node. Using this condition and those from Table 2.1, the third- and fourth-order polynomials become

$$P_3(x) = v(1-v)(v-.5) \qquad 2.2d$$

and

$$P_4(x) = v(1-v)(v^2 - v + .2). \qquad 2.2e$$

Table 2.1 Value of polynomials when evaluated at node edges and when integrated over the node width. Adapted from reference number 4.

	X_i	X_{i+1}	$\int dx$
$P_{\bar{\Phi}}$	0	0	1
P_{Φ^-}	1	0	0
P_{Φ^+}	0	1	0
P_3	0	0	0
P_4	0	0	0

2.3 Derivation of the Nodal Equations for Inner Nodes

In a one-dimensional system, the nodal equations relate the parameter of interest in node i to the parameter in the nodes on either side, nodes i+1 and i-1. For this reason, the nodal equations for the outer two nodes, nodes 1 and N, must be derived separately from those for the inner nodes. Section 2.4 details the derivation for the outer nodes while this section considers the inner nodes.

2.3.1 Derivation of the Flux Nodal Equation

Integration of the Boltzmann transport equation over all directions and over energy group g results in the multigroup neutron conservation equation[2]. This equation in one-dimensional form is

$$\frac{d}{dx}J_g(x) + \Sigma_g(x)\Phi_g(x) = \sum_{g'=1}^{G} \frac{1}{\lambda}\chi_g \nu\Sigma_{fg'}(x)\Phi_{g'}(x)$$

$$+ \sum_{g'=1,g'\neq g}^{G} \Sigma_{gg'}(x)\Phi_{g'}(x) \qquad g=1,2,...,G \qquad 2.3$$

where

$J_g(x)$ - net current density in group g,

$\Sigma_g(x)$ - total macroscopic removal cross-section for group g,

$\Phi_g(x)$ - scalar flux density in group g,

λ - multiplication factor, k-effective,

χ_g - fraction of fission neutrons emitted in group g,

$\nu\Sigma_{fg}(x)$ - number of fission neutrons emitted per fission times the macroscopic fission cross-section for group g,

$\Sigma_{gg'}(x)$ - macroscopic scattering cross-section from group g' to group g,

and

G - number of energy groups.

The right-hand side of Eqn. 2.3 is the source of neutrons in group g and will be replaced by $S_g(x)$.

Integration of Eqn 2.3 over the width of node i gives the nodal balance equation

$$J_g(x_{i+1}) - J_g(x_i) + \Sigma_g^i h_i \overline{\Phi}_g^i = S_g^i \qquad 2.4$$

where

$J_g(x_{i+1})$ - net current density at x_{i+1} for group g,

$J_g(x_i)$ - net current density at x_i for group g,

Σ_g^i - total macroscopic removal cross-section for group g in node i,

$\bar{\Phi}_g^i$ - average group g flux in node i,

and

S_g^i - source of group g neutrons in node i.

In order to solve this equation (which contains two unknowns, the flux and the current density) a second relation is needed. This relation is obtained by using Fick's Law. In one-dimensional, energy group form Fick's Law becomes

$$J_g(x) = -D_g \frac{d}{dx}\Phi_g(x)$$

where

D_g - diffusion coefficient for group g.

When Eqns. 2.1 and 2.2 are substituted for $\Phi_g(x)$, the previous equation becomes

$$J_g(x) = -D_g^i\left[\frac{6}{h_i}(1-2v)\bar{\Phi}_g^i - \frac{2}{h_i}(2-3v)\Phi_g^i + \frac{2}{h_i}(3v-1)\Phi_g^{i+1} - \frac{1}{h_i}(3v^2 - 3v + .5)C_{3g}^i\right]$$

$$-D_g^i\left(\frac{1}{h_i}\right)(1-2v)(2v^2 - 2v + .2)C_{4g}^i \qquad 2.5$$

where

D_g^i - diffusion coefficient in node i for group g.

Now that the two relations between the current density and the flux have been determined, it is a matter of algebraic manipulation that leads to the nodal equation for the flux. The manipulation procedure is outlined below.

1. Using Eqn 2.5, the sum of $J_g(x_i)$ and $J_g(x_{i+1})$ is determined for node i.

2. By combining the result of Step 1 with Eqn. 2.4, $J_g(x_{i+1})$ can be eliminated and a relation between $J_g(x_i)$ and the

coefficients in the flux expansion can be determined.

3. After using Eqn. 2.5 to determine $J_g(x_i)$, the equation is used to eliminate Φ_g^{i+1} from the result of Step 2.

4. Repeating Steps 1,2, and 3 for node i-1 results in a second equation for $J_g(x_i)$.

5. Using the result of Step 4 to eliminate Φ_g^i from the result of Step 3, an equation relating $J_g(x_i)$ to the average group flux and the third- and fourth-order coefficients for nodes i and i-1 is obtained

6. The final step is to use the result of Step 5 to construct $J_g(x_i)$ and $J_g(x_{i+1})$ and put these relations into Eqn. 2.4.

After these steps are carried out and the equation simplified, the nodal equation for the node average group flux in the inner nodes takes the form

$$(K_{1g}^i + K_{1g}^{i+1})K_{3g}^i\bar{\Phi}_g^i + \Sigma_g^i h_i\bar{\Phi}_g^i - K_{1g}^i K_{3g}^{i-1}\bar{\Phi}_g^{i-1} - K_{1g}^{i+1}K_{3g}^{i+1}\bar{\Phi}_g^{i+1} =$$

$$\left|1 - \frac{1}{3}\frac{h_i}{D_g^i}(K_{1g}^i + K_{1g}^{i+1})\right|S_g^i + \frac{h_{i-1}}{3D_g^{i-1}}K_{1g}^i S_g^{i-1} + \frac{h_{i+1}}{3D_g^{i+1}}K_{1g}^{i+1}S_g^{i+1}$$

$$- \frac{1}{15}(K_{1g}^i + K_{1g}^{i+1})C_{4g}^i + \frac{1}{15}K_{1g}^i C_{4g}^{i-1} + \frac{1}{15}K_{1g}^i C_{4g}^{i+1}$$

$$+ \frac{1}{2}(K_{1g}^i - K_{1g}^{i+1})C_{3g}^i + \frac{1}{2}K_{1g}^i C_{3g}^{i-1} - \frac{1}{2}K_{1g}^{i+1}C_{3g}^{i+1} \qquad i=2, 3,...,N-1 \qquad 2.6$$

where

$$K_{1g}^i = \left(\frac{h_i}{D_g^i} + \frac{h_{i-1}}{D_g^{i-1}}\right)^{-1} \qquad K_{3g}^i = \left(2 - \frac{1}{3}\frac{h_i^2}{D_g^i}\Sigma_g^i\right)$$

$$S_1^i = \frac{1}{\lambda}\left(\nu\Sigma_{f1}^i\bar{\Phi}_1^i + \nu\Sigma_{f2}^i\bar{\Phi}_2^i\right)h_i \qquad S_2^i = h_i\Sigma_{21}^i\bar{\Phi}_1^i$$

N - number of nodes.

The source terms reduce to the relations above because of the assumptions of no up-scatter and that all fission neutrons appear in group 1.

2.3.2 Derivation of Third- and Fourth-Order Expansion Coefficient Nodal Equations

A weighted residual method[2] is used in the derivation of the expansion coefficient nodal equations. Because there are two unknown constants, two linearly independent weight functions are used. The weight functions used are $(v - .5)$ and $(3v^2 - 3v + .5)$.

The derivation proceeds by substituting Eqns. 2.1 and 2.2 into Eqn. 2.3, with the right-hand side replaced by $S_g(x)$. This equation is then multiplied by the weight function and integrated over the node width (x from x_i to x_{i+1} or v from 0 to 1). At this point, the equations for the two energy groups must be treated separately because of the difference in the source terms. The difference is made apparent by the use of the weight functions. The resulting equations

$$\left(\frac{1}{2h_i} D_1^i - \frac{1}{20} h_i\Sigma_1^i + \frac{1}{20}\frac{\nu\Sigma_{f1}^i}{\lambda} h_i\right) C_{31}^i + \frac{1}{20}\frac{\nu\Sigma_{f2}^i}{\lambda} h_i C_{32}^i$$
$$= \frac{1}{24}\frac{h_i^2}{D_1^i}\left(\frac{\nu\Sigma_{f1}^i}{\lambda} - \Sigma_1^i\right)(J_1^{i+1} + J_1^i) + \frac{1}{24}\frac{h_i^2}{D_2^i}\frac{\nu\Sigma_{f2}^i}{\lambda}(J_2^{i+1} + J_2^i), \qquad 2.7$$

$$\left(\frac{1}{5h_i} D_1^i - \frac{1}{210} h_i\Sigma_1^i + \frac{1}{210}\frac{\nu\Sigma_{f1}^i}{\lambda} h_i\right) C_{41}^i + \frac{1}{210}\frac{\nu\Sigma_{f2}^i}{\lambda} h_i C_{42}^i$$
$$= \frac{1}{120}\frac{h_i^2}{D_1^i}\left(\frac{\nu\Sigma_{f1}^i}{\lambda} - \Sigma_1^i\right)(J_1^{i+1} - J_1^i) + \frac{1}{120}\frac{h_i^2}{D_2^i}\frac{\nu\Sigma_{f2}^i}{\lambda}(J_2^{i+1} - J_2^i), \qquad 2.8$$

$$\frac{1}{20} h_i\Sigma_{21}^i C_{31}^i + \left(\frac{1}{2h_i} D_2^i - \frac{1}{20} h_i\Sigma_2^i\right) C_{32}^i$$
$$= \frac{1}{24}\frac{h_i^2}{D_1^i}\Sigma_{21}^i(J_1^{i+1} + J_1^i) - \frac{1}{24}\frac{h_i^2}{D_2^i}\Sigma_2^i(J_2^{i+1} + J_2^i), \qquad 2.9$$

and

$$\frac{1}{210} h_i\Sigma_{21}^i C_{41}^i + \left(\frac{1}{5h_i} D_2^i - \frac{1}{210} h_i\Sigma_2^i\right) C_{42}^i$$

$$= \frac{1}{120}\frac{h_1^2}{D_1^i}\Sigma_{21}^i(J_1^{i+1} - J_1^i) - \frac{1}{120}\frac{h_1^2}{D_2^i}\Sigma_2^i(J_2^{i+1} - J_2^i) \qquad 2.10$$

where $J_g^i = J_g(x_i)$

relate the current density at the node surfaces to the expansion coefficients. The (v-.5) weighted equations, Eqns. 2.7 and 2.9, are independent of the fourth-order coefficient and are additive in the currents whereas the other equations, Eqns. 2.8 and 2.10, are independent of the third-order coefficient and are difference equations in the currents. Note that Eqns. 2.7, 2.8, 2.9, and 2.10 are dependent on node i quantities only and, therefore, are valid for all nodes.

Two more equations are needed, in addition to Eqns. 2.7, 2.8, 2.9, and 2.10, that relate the current densities to the expansion coefficients for system closure. The first equation is formed by summing $J_g(x_i)$ and $J_g(x_{i+1})$, formed from the result of Step 5 Subsection 2.3.1. The nodal equation for the sum of the edge currents for node i is

$$\begin{aligned} J_g(x_{i+1}) + J_g(x_i) = {} & (K_{1g}^{i+1} - K_{1g}^i)K_{3g}^i\Phi_g^i + K_{1g}^iK_{3g}^{i-1}\Phi_g^{i-1} - K_{1g}^{i+1}K_{3g}^{i+1}\Phi_g^{i+1} \\ & + \frac{h_i}{3D_g^i}(K_{1g}^{i+1} - K_{1g}^i)S_g^i + \frac{h_{i-1}}{3D_g^{i-1}}K_{1g}^iS_g^{i-1} - \frac{h_{i+1}}{3D_g^{i+1}}K_{1g}^{i+1}S_g^{i+1} \\ & + \frac{1}{2}(K_{1g}^i + K_{1g}^{i+1})C_{3g}^i + \frac{1}{2}K_{1g}^{i+1}C_{3g}^{i+1} + \frac{1}{2}K_{1g}^iC_{3g}^{i-1} \\ & + \frac{1}{15}(K_{1g}^{i+1} - K_{1g}^i)C_{4g}^i + \frac{1}{15}K_{1g}^iC_{4g}^{i-1} - \frac{1}{15}K_{1g}^{i+1}C_{4g}^{i+1} \qquad i=2,\ldots,N-1 \quad 2.11 \end{aligned}$$

The second equation, a difference equation in $J_g(x_{i+1})$ and $J_g(x_i)$, is the nodal balance equation, Eqn. 2.4.

2.4 Boundary Conditions and Derivation of the Nodal Equations For Outer Nodes

2.4.1 Boundary Conditions

The boundary condition imposed is that the current in the x-direction at the edge of the reactor equals to a constant, the albedo, times the flux at the edge. In energy group form and for the right and left edges of the reactor, the boundary conditions take the form

$$J_g(x_R) = \alpha_{gR}\Phi_g(x_R)$$

and

$$J_g(x_L) = -\alpha_{gL}\Phi_g(x_L)$$

where

α_{gL} - albedo for the left edge and group g

and

α_{gR} - albedo for the right edge and group g.

With this form, the boundary condition can range from zero net current (alpha equals zero) to zero flux (alpha is large) at the reactor boundaries.

2.4.2 Derivation of the Flux Nodal Equation for Node N

The steps in the manipulation of the equations in Subsection 2.3.1 that result in the nodal equation for the flux in the furthest right node, node N, are as follows:

1. Eqn. 2.5 is used to determine $J_g(x_R)$ where i=N, i+1=R, and v=1.

2. The boundary condition is used to eliminate Φ_g^R from the result of Step 1.

3. The sum of $J_g(x_R)$ and $J_g(x_N)$ are determined using

Eqn. 2.5.

4. The boundary condition is used to eliminate Φ_g^R from the result of Step 3.

5. Eqn. 2.4 written for node N is used to eliminate $J_g(x_N)$ from the result of Step 4.

6. Φ_g^N is eliminated from the previous result using the result of Step 2.

7. Step 5 from Subsection 2.3.1 is used to determine $J_g(x_N)$. This relation and that resulting from Step 6 above are substituted into Eqn. 2.4 written for node N.

After rearranging terms, the nodal equation for the node average group flux is

$$\left(\frac{3}{h_N} K_{3g}^N K_{4g}^N + K_{3g}^N K_{1g}^N + \Sigma_g^N h_N\right)\bar{\Phi}_g^N - K_{3g}^{N-1} K_{1g}^N \bar{\Phi}_g^{N-1}$$

$$= \left(1 - \frac{1}{D_g^N} K_{4g}^N - \frac{1}{3}\frac{h_N}{D_g^N} K_{1g}^N\right) S_g^N + \frac{1}{3}\frac{h_{N-1}}{D_g^{N-1}} K_{1g}^N S_g^{N-1}$$

$$- \left(\frac{1}{5h_N} K_{4g}^N + \frac{1}{15} K_{1g}^N\right) C_{4g}^N + \frac{1}{15} K_{1g}^N C_{4g}^{N-1}$$

$$+ \left(\frac{-3}{2h_N} K_{4g}^N + \frac{1}{2} K_{1g}^N\right) C_{3g}^N + \frac{1}{2} K_{1g}^N C_{3g}^{N-1} \qquad 2.12$$

where

$$K_{4g}^N = \alpha_{gR}\left(\frac{3\alpha_{gR}}{D_g^N} + \frac{6}{h_N}\right)^{-1}.$$

2.4.3 Derivation of the Flux Nodal Equation for Node 1

The steps in the manipulation of the equations in Subsection 2.3.1 that result in the nodal equation for the flux in the furthest left node, node 1, are as follows:

1. Eqn. 2.5 is used to determine $J_g(x_{i+1})$ where i=1, i+1=2,

and v=0.

2. The boundary condition is used to eliminate Φ_g^1 from the result of Step 1.

3. The sum of $J_g(x_1)$ and $J_g(x_2)$ are determined using Eqn. 2.5.

4. The boundary condition is used to eliminate Φ_g^1 from the result of Step 3.

5. Eqn. 2.4 written for node 1 is used to eliminate $J_g(x_2)$ from the result of Step 4.

6. Φ_g^2 is eliminated from the previous result using the result of Step 2.

7. Step 5 from Subsection 2.3.1 is used to determine $J_g(x_2)$. This relation and that resulting from Step 6 above are substituted into Eqn. 2.4 written for node 1.

After rearranging terms, the nodal equation for the node average group flux is

$$\left(\frac{3}{h_1} K_{3g}^1 K_{4g}^1 + K_{3g}^1 K_{1g}^2 + \Sigma_g^1 h_1\right)\overline{\Phi}_g^1 - K_{3g}^2 K_{1g}^2 \overline{\Phi}_g^2$$

$$= \left(1 - \frac{1}{D_g^1} K_{4g}^1 - \frac{1}{3}\frac{h_1}{D_g^1} K_{1g}^2\right) S_g^1 + \frac{1}{3}\frac{h_2}{D_g^2} K_{1g}^2 S_g^2$$

$$- \left(\frac{1}{5h_1} K_{4g}^1 + \frac{1}{15} K_{1g}^2\right) C_{4g}^1 + \frac{1}{15} K_{1g}^2 C_{4g}^2$$

$$+ \left(\frac{3}{2h_1} K_{4g}^1 - \frac{1}{2} K_{1g}^2\right) C_{3g}^1 - \frac{1}{2} K_{1g}^2 C_{3g}^2 \qquad 2.13$$

where

$$K_{4g}^1 = \alpha_{gL}\left(\frac{3\alpha_{gL}}{D_g^1} + \frac{6}{h_1}\right)^{-1}.$$

2.4.4 Derivation of the Expansion Coefficient Nodal Equations in Node N

The nodal equations for the third- and fourth-order expansion coefficients, Eqns. 2.7, 2.8, 2.9, and 2.10, depend only on node i quantities. For this reason, the expansion coefficient nodal equations for node N do not need to de derived separately.

However, Eqn. 2.11, the sum of the current on each side of the node, depends on the node of interest and the two neighboring nodes. Equation 2.11 is therefore not valid for node N. For this reason, a relation valid in node N must be derived. This relation is formed by summing $J_g(x_R)$, formed from the result of Step 6 Subsection 2.4.2, and $J_g(x_N)$ for node N, formed from the result of Step 5 Subsection 2.3.1. The nodal equation for the sum of the edge currents for node N is

$$J_g(x_R) + J_g(x_N) = \left(\frac{3}{h_N} K_{4g}^N - K_{1g}^N\right) K_{3g}^N \bar{\Phi}_g^N + K_{1g}^N K_{3g}^{N-1} \bar{\Phi}_g^{N-1}$$

$$- \left(-\frac{1}{D_g^N} K_{4g}^N + \frac{h_N}{3D_g^N} K_{1g}^N\right) S_g^N + \frac{h_{N-1}}{3D_g^{N-1}} K_{1g}^N S_g^{N-1} + \left(\frac{3}{2h_N} K_{4g}^N + \frac{1}{2} K_{1g}^N\right) C_{3g}^N$$

$$+ \frac{1}{2} K_{1g}^N C_{3g}^{N-1} + \left(\frac{1}{5h_N} K_{4g}^N - \frac{1}{15} K_{1g}^N\right) C_{4g}^N + \frac{1}{15} K_{1g}^N C_{4g}^{N-1} \qquad 2.14$$

2.4.5 Derivation of the Expansion Coefficient Nodal Equations for Node 1

The nodal equations for the third- and fourth-order expansion coefficients, Eqns. 2.7, 2.8, 2.9, and 2.10, depend only on node i quantities. For this reason, the expansion coefficient nodal equations for node 1 do not need to de derived separately.

However, Eqn. 2.11, the sum of the current on each side of the node, depends on the node of interest and the two neighboring nodes. Equation 2.11 is therefore not valid in node 1. For this reason, a relation valid for node 1 must be derived. The relation is formed by summing $J_g(x_1)$, formed from the result of Step 6 Subsection 2.4.3, and $J_g(x_2)$

for node 1, formed from the result of Step 5 Subsection 2.3.1. The nodal equation for the sum of the edge currents for node 1 is

$$J_g(x_1) + J_g(x_2) = (-\frac{3}{h_1} K^1_{4g} + K^1_{1g})K^1_{3g}\overline{\Phi}^1_g - K^2_{1g}K^2_{3g}\overline{\Phi}^2_g + (-\frac{1}{D^1_g} K^1_{4g} + \frac{h_1}{3D^1_g} K^2_{1g})\, S^1_g$$

$$- \frac{h_2}{3D^2_g} K^2_{1g}\, S^2_g + (\frac{3}{2h_1} K^1_{4g} + \frac{1}{2}K^2_{1g})\, C^1_{3g} + \frac{1}{2}K^2_{1g}C^2_{3g}$$

$$+ (\frac{-1}{5h_1} K^1_{4g} + \frac{1}{15}K^2_{1g})\, C^1_{4g} - \frac{1}{15}K^2_{1g}C^2_{4g} \qquad 2.15$$

2.5 Summary

The derivation of the nodal equations for a one-dimensional, two energy-group system has been presented in this chapter. These equations provide relations for the calculation of the node average group flux, the third-order expansion coefficient, and the fourth-order expansion coefficient in each node.

Chapter 3 describes the method used to solve these nodal equations in order to obtain the node average group flux for the system of interest.

Chapter 3

SOLUTION METHOD

3.1 Introduction

This chapter covers the second step in the work performed, the determination of the solution method. Since the nodal equations for the node average group fluxes involve quantities from the node of interest and neighboring nodes, the solution of these equations starts by forming matrix relations. Matrix equations are not necessary when solving for the third- and fourth-order expansion coefficients since the nodal equations only contain quantities for a single node.

A double iteration scheme is used to obtain the node average fluxes from the six nodal equations. This scheme is necessary since the flux depend on the expansion coefficients and the expansion coefficients, through the edge current relations, depend on the fluxes.

3.2 Matrix Relations

In order to solve the nodal equations derived in Chapter 2, the equations for the node-average group-fluxes are written in matrix form. Equation 2.6 for group g takes the form

$$[A_g]\,[\bar{\Phi}_g] = [B_g]\,[S_g] + [H_g]\,[C_{3g}] + [L_g]\,[C_{4g}] \qquad 3.1$$

where

$[A_g]$, $[B_g]$, $[H_g]$, and $[L_g]$ - tridiagonal NxN matrices of group g material constants,

$[\bar{\Phi}_g]$ - column vector of length N of the node average flux for group g,

$[S_g]$ - column vector of length N of the neutron source for group g,

$[C_{3g}]$ - column vector of length N of the third-order expansion coefficient for group g,

and

$[C_{4g}]$ - column vector of length N of the fourth-order expansion coefficient for group g.

The matrices and column vectors in Eqn. 3.1 are formed by writing each row for a different node i. Equations 2.13 and 2.12, respectively, are used when relations for nodes 1 and N are required. Equation 2.6 is the relation for nodes 2 through N-1.

3.3 Solution Scheme

The quantity of interest is the node average group flux. However, this flux is dependent on two unknown variables, the source and the expansion coefficients. Both of these variables are dependent on the flux and the expansion coefficients are also dependent on the source. Because of this circular relationship a double iteration solution scheme is necessary.

3.3.1 Flux Iteration

The flux iteration involves the convergence of the flux and k-effective for fixed expansion coefficients[5]. Equation 3.1 shows that the node average flux depends only on the source when the expansion coefficients are fixed. The source, however, is dependent on the flux (see Subsection 2.3.1) so an iteration is necessary. Using iteration notation, the relations to be solved for group g are of the form

$$[S^i] = [M]\,[\bar{\Phi}^i]$$

and

$$[A]\,[\bar{\Phi}^{i+1}] = [B]\,[S^i] + K$$

where

$[\bar{\Phi}^{i+1}]$ - node average flux from flux iteration i+1,

$[S^i]$ - neutron source from flux iteration i,

$[A]$, $[B]$, $[M]$ - matrices of material constants

and

K - constant.

In order to solve for the fluxes using equations in the form of Eqn. 3.1, a forward-elimination backward-substitution scheme is used.

The flux iteration continues until either a maximum number of iterations is reached or the flux and the k-effective converge[5], whichever is sooner. The equations for the convergence criteria are

$$\frac{\lambda^{i+1} - \lambda^{i}}{\lambda^{i+1}} < \varepsilon_{\lambda} \qquad 3.2$$

and

$$\max \left| \frac{\bar{\Phi}^{i+1} - \bar{\Phi}^{i}}{\bar{\Phi}^{i+1}} \right| < \varepsilon_{\Phi} \qquad 3.3$$

where

i - flux iteration number,

ε_{λ} - k-effective convergence criteria,

and

ε_{ϕ} - node average flux convergence criteria.

3.3.2 Quartic Expansion Coefficient Iteration

The quartic expansion coefficient iteration involves the updating of the expansion coefficients and the node edge currents. An iteration to determine the expansion coefficients is not necessary since the fourth-order expansion coefficient nodal equations are independent of the third-order expansion coefficients and vice versa . Before updating the expansion coefficients, the sum and difference of the node edge currents must be updated using Eqns. 2.4, 2.11, 2.14, and 2.15. The flux and source that are used on the right-hand-side of Eqns. 2.4, 2.11, 2.14, and 2.15 are the converged flux from the flux iteration and the source that produced that flux.

Flux and k-effective convergence criteria[5] are used to determine when the quartic expansion coefficient iteration is complete. The equations for the two criteria are same as those for the flux iteration, Eqns. 3.2 and 3.3, with i replaced by i_0 where i_0 is the quartic expansion coefficient iteration number.

3.3.3 Iteration Summary

Figure 3.1 shows the flow of the solution schematically. This figure shows that the flux loop is inside of the quartic expansion coefficient loop. Also it shows that there are two ways that the flux iteration can be stopped, either by reaching a maximum number of iterations or obtaining convergence. The expansion coefficient iteration is stopped only after convergence is obtained.

3.4 Summary

The solution method to be used has been presented in this chapter. Because of the form of the nodal equations as derived in Chapter 2, the method involves a double iteration. Two convergence criteria are used to determine when the calculation is complete. Both the k-effective and the node average flux are converged.

Chapter 4 details the final part of the work, the application of the solution method presented in this chapter.

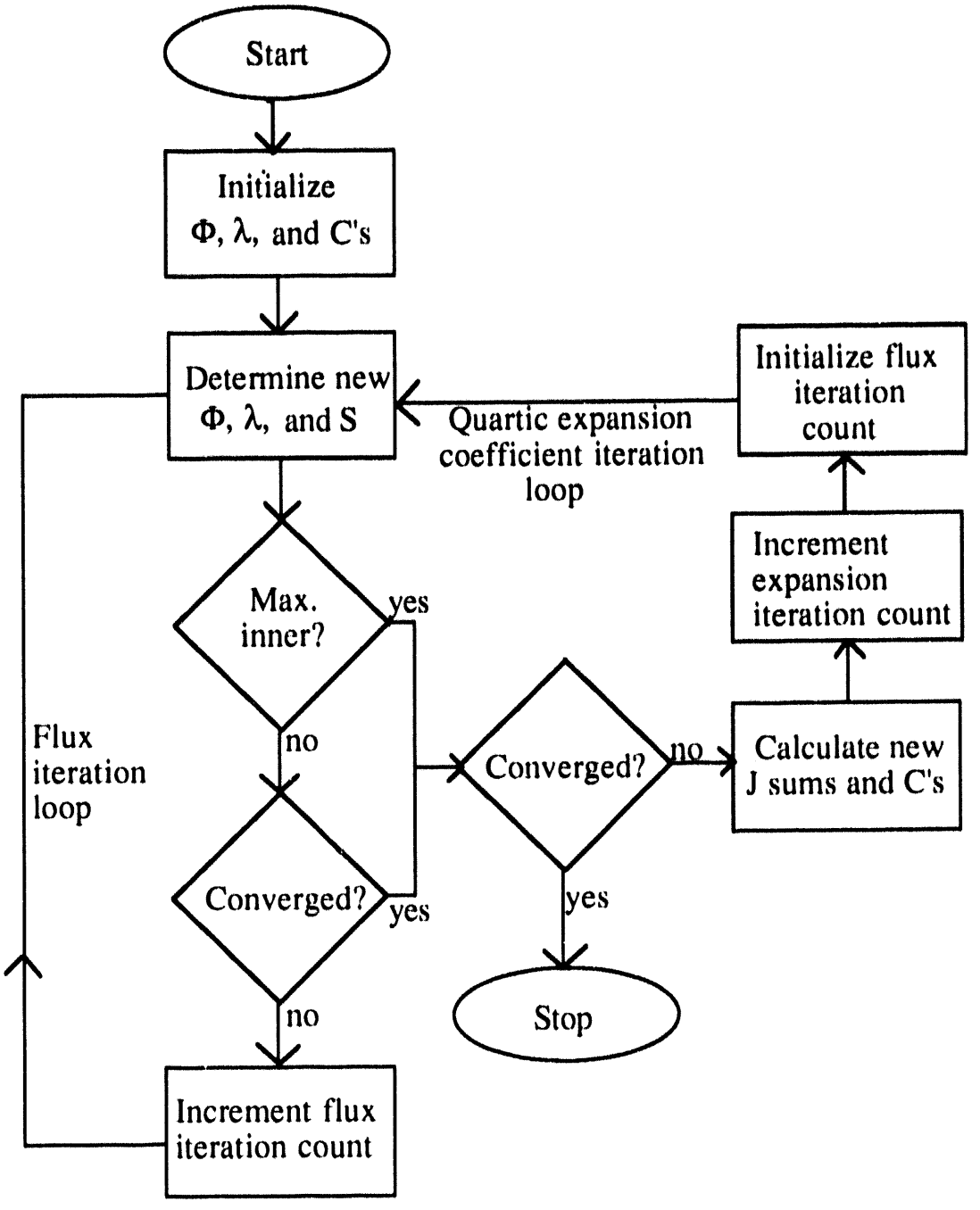

Figure 3.1 Schematic of iteration loops.

Chapter 4

APPLICATION OF SOLUTION METHOD

4.1 Introduction

The application of the solution method developed in the previous chapter is presented in this chapter. Because the solution method involves two iteration loops and coupled equations (coupled by nodes), the solution was automated.

Before the computer programs were applied to any test cases, they were benchmarked. The benchmark used is the International Atomic Energy Agency (IAEA) Light Water Reactor (LWR) Benchmark Problem.

Three types of reactors are modeled and used to examine the usefulness of the quadratic flux shape approximation in energy group one and quartic flux shape approximation in energy group two. The results of the two computer programs for graphite reactor, pressurized water reactor, and heavy water reactor test problems were compared.

4.2 Computer Programs

The solution method described in Chapter 3 was carried out through the use of Project Athena, the M.I.T. computer network. A computer program was written based on the equations in Chapter 2 written in the form of a matrix equation and a set of algebraic equations. This program was written in FORTRAN 77 using single precision variables. Figure 4.1 shows the flow of the computer program schematically.

The program as written, using the equations in Chapter 2, is for a fourth-order flux shape approximation in both energy groups. This program is named Fourfour.f.

In order to obtain a program for a second-order flux shape approximation in energy group one and a fourth-order flux shape approximation in energy group two, Fourfour.f was modified and named Twofour.f.

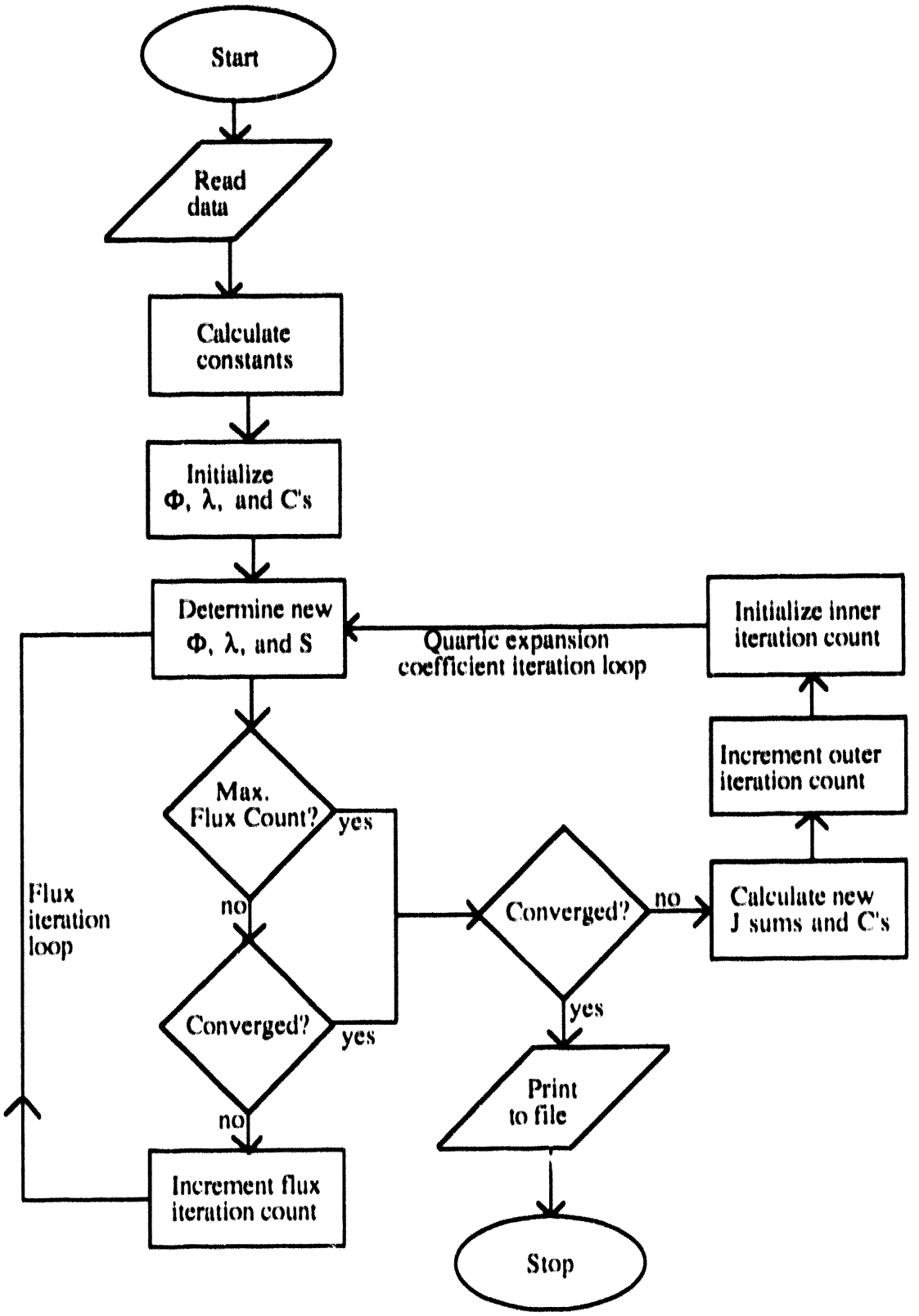

Figure 4.1 Computer program flowchart.

Two modifications were made to obtain the second program. First, the third- and fourth-order flux expansion coefficients were set to zero for energy group one in the flux and sum of current equations, Eqns. 2.6, 2.11, 2.12, 2.13, 2.14, and 2.15. And second, the expansion coefficient equations derived using the group one flux expansion, Eqns. 2.7 and 2.8, were eliminated.

4.3 Benchmark Problem

The benchmark problem used was the Three-dimensional LWR Problem (3D IAEA Benchmark Problem). This problem is based on two-group diffusion theory with no net current at symmetry boundaries and no incoming current at external boundaries. Because the computer programs written for this thesis are for one-dimensional systems, a slice in the x-direction at y=0 and z=0 was used to test the programs. Node sizes of 20 cm, 10 cm, and 5 cm were used in the benchmarking of the programs.

The results from runs of Fourfour.f at the three node sizes were compared with the results of the identical problems run by a more general code[5]. Agreement to four places, variation of less than one ten-thousandth, was seen in the eigenvalue. The shape of the flux for each energy group from Fourfour.f was within one percent of the results from the more general code.

The results from runs of Twofour.f at the 20 cm node size were compared with the results of the identical problem run by a more general code[5]. Agreement to four places, variation of less than one ten-thousandth, was seen in the eigenvalue. The shape of the flux for each energy group from Twofour.f was within one percent of the results from the more general code.

4.4 Test Problems

4.4.1 Graphite Reactor

The test problem used to model a graphite reactor was a slice of a General Atomics MHTGR. The one-dimensional slice used contains each of the five regions that make up the MHTGR core: four reflector regions and one region containing fissile material. Figure 4.2 shows the order of the regions in the slice used. The macroscopic cross sections corresponding to each region in Fig. 4.2 are given in Table 4.1. The boundary conditions used are zero flux at the center of the core and no incoming current at the external edge of the core.

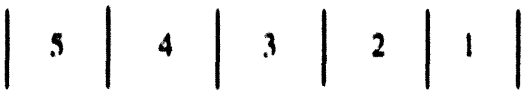

Figure 4.2 MHTGR model. Region 1 is 82.6 cm wide, region 2 is 92.1 cm wide, region 3 is 33.8 cm wide, region 4 is 33.5 cm wide, and region 5 is 54.9 cm wide. Symmetry boundary conditions on the right.

Table 4.2 gives the percent difference in the node-average fluxes for the two approximate models (second-order flux shape approximation in energy group one combined with a fourth-order approximation in energy group two and a fourth-order approximation in both energy groups). The nodes are numbered from left to right across the model shown in Fig. 4.2. Node sizes of 13.73 cm in region 5, 8.37 cm in region 4, 8.45 cm in region 3, 11.51 cm in region 2, and 10.33 cm in region 1 were used to obtain the results given. These node sizes were used because it was determined that Fourfour.f gave accurate results for the MHTGR for this node spacing.

Table 4.1 Macroscopic cross sections for graphite reactor.

Region	Group	D_g (cm)	$\nu\Sigma_{fg}$ (cm^{-1})	Σ_g (cm^{-1})	$\Sigma_{gg'}$ (cm^{-1})
1	1	1.14393	0.0	4.08940×10^{-3}	4.08173×10^{-3}
	2	0.863447	0.0	1.55156×10^{-4}	
2	1	1.49750	3.46297×10^{-4}	3.32021×10^{-3}	2.37932×10^{-3}
	2	1.15689	5.89872×10^{-3}	3.37634×10^{-3}	
3	1	1.79242	0.0	2.61068×10^{-3}	2.60554×10^{-3}
	2	1.31833	0.0	1.10976×10^{-4}	
4	1	1.10933	0.0	4.21826×10^{-3}	4.20995×10^{-3}
	2	0.815916	0.0	1.79312×10^{-4}	
5	1	1.05650	0.0	4.42917×10^{-3}	4.42045×10^{-3}
	2	0.777063	0.0	1.88278×10^{-4}	

Table 4.2 shows that the eigenvalue from the unmixed approximation is 0.13% smaller than the eigenvalue from the mixed approximation (second-order flux shape approximation in energy group one and a fourth-order approximation in energy group two). This fact suggests that the use of the mixed approximation for this problem is advantageous (results in little accuracy loss).

The difference in the node-average fluxes from the two approximate models ranges from -0.6% to 12.1% in energy group one and -0.3% to 1.8% in energy group two. The energy group two values again suggest that the use of the mixed approximation for this problem is advantageous. For energy group one, Table 4.2 shows that the difference in the fluxes in the fuel region, nodes 13 through 20, are all less than 1% in absolute value. Also, the large values (greater than 5%) of the differences in energy group one occur in the outermost

reflector and the center of the innermost reflector. These two facts, for energy group one, combined suggest that the use of the mixed approximation is advantageous.

Based on the differences in the node-average fluxes from both energy groups and the eigenvalue difference, the use of the mixed approximation when applied to the MHTGR is advantageous.

Table 4.2 Comparison of the node-average flux value for each node for the MHTGR. The values from Fourfour.f are larger by the percentage given.

Node	Group 1	Group 2	Node	Group 1	Group 2
1	12.1%	1.8%	15	-0.6%	-0.2%
2	9.7%	1.7%	16	-0.5%	-0.3%
3	7.1%	1.7%	17	-0.5%	-0.3%
4	4.1%	1.6%	18	-0.4%	-0.2%
5	3.3%	1.6%	19	-0.1%	0.02%
6	3.1%	1.5%	20	0.6%	0.3%
7	2.7%	1.4%	21	1.6%	0.7%
8	2.1%	1.3%	22	2.6%	1.0%
9	1.9%	1.2%	23	3.6%	1.2%
10	1.9%	1.1%	24	4.5%	1.4%
11	1.8%	1.1%	25	5.4%	1.5%
12	1.7%	0.9%	26	6.0%	1.6%
13	0.7%	0.6%	27	6.0%	1.6%
14	-0.3%	0.1%	28	6.4%	1.7%
Eigenvalue difference -0.13%					

Figure 4.3 shows a plot of the flux as a function of position in each energy group for the two approximate models. The position increases from left to right across the model shown in Fig. 4.2. The plot for energy group one in Fig. 4.3 shows that the flux from the two approximate models are essentially the same. This is also the case for energy group two. The flux from the two approximate models is essentially the same in Fig. 4.3 for energy group two.

Figure 4.3

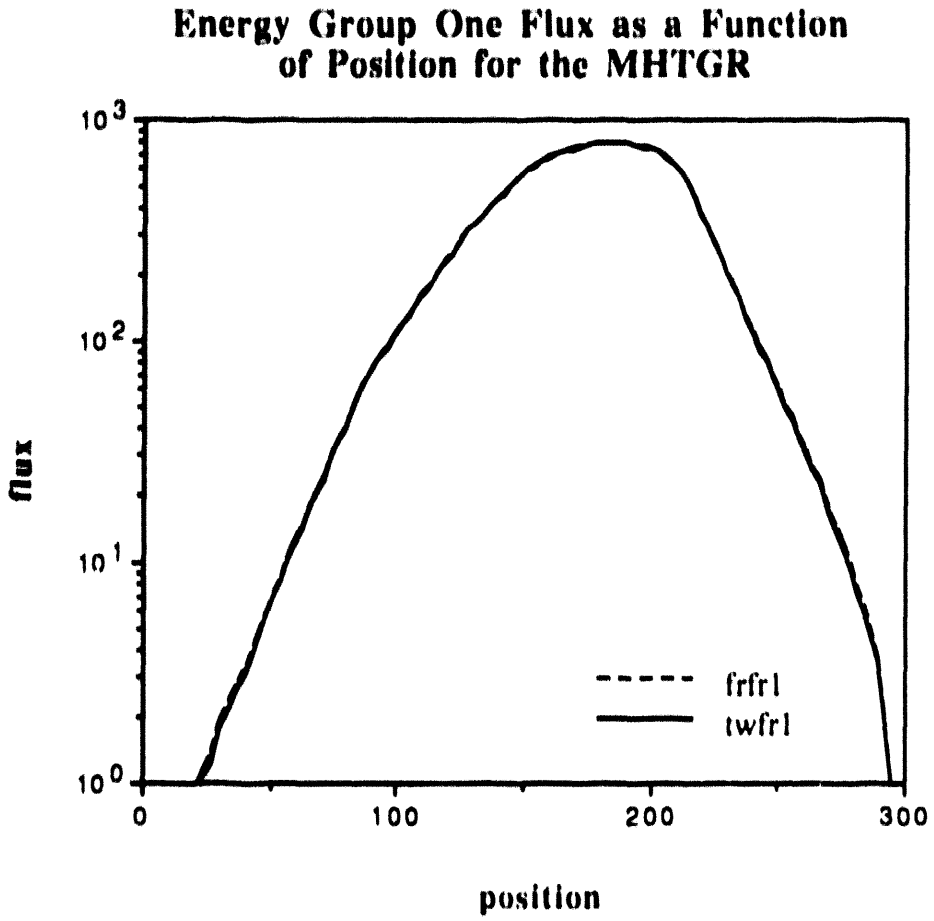

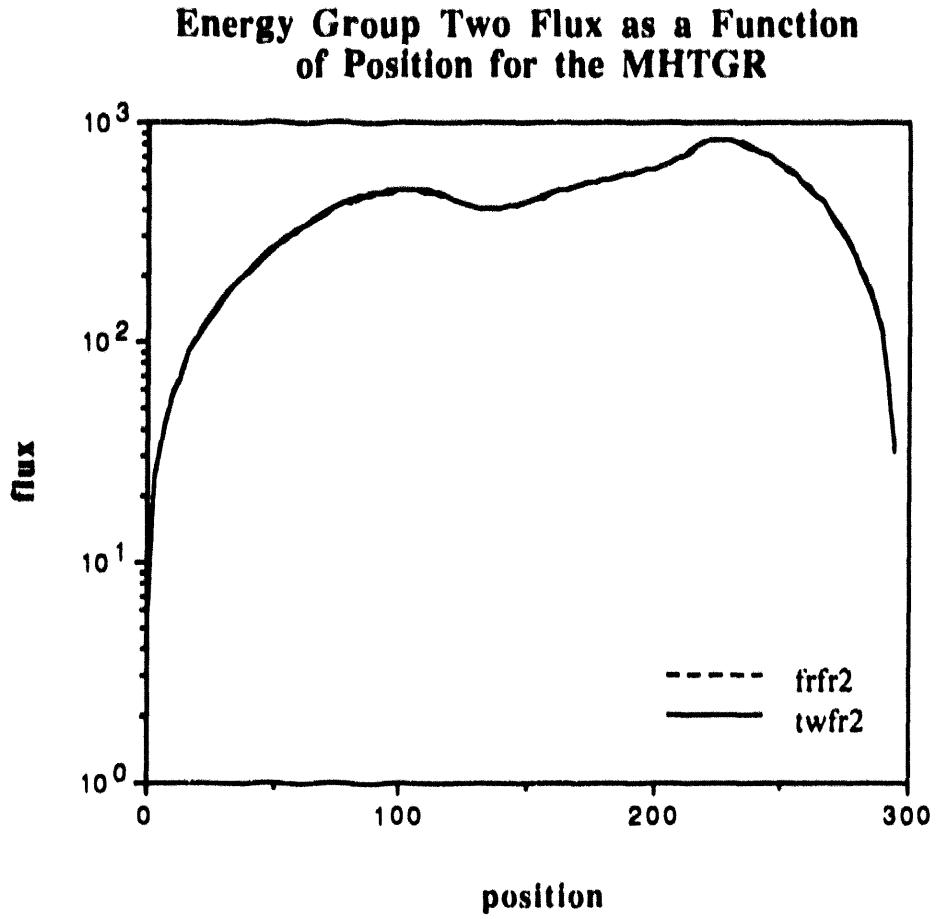

4.4.2 Pressurized Light Water Reactor

The test problem used to model a PWR was a slice of the Salem - 1 core. Four one-dimensional slices were used. Two slices were in the x-direction at z = 0 and the other two were in the z-direction at y = 0. Figure 4.4 shows the order of the compositions in the four slices used. The macroscopic cross sections corresponding to the compositions in Fig. 4.4 are given in Table 4.3. The boundary conditions used for the slices in the x-direction are no net current at the center of the core and no incoming current at the external edge of the core. The boundary conditions used for the slices in the z-direction are an albedo of 0.24931 for energy group one and an albedo of 0.11119 for energy group two.

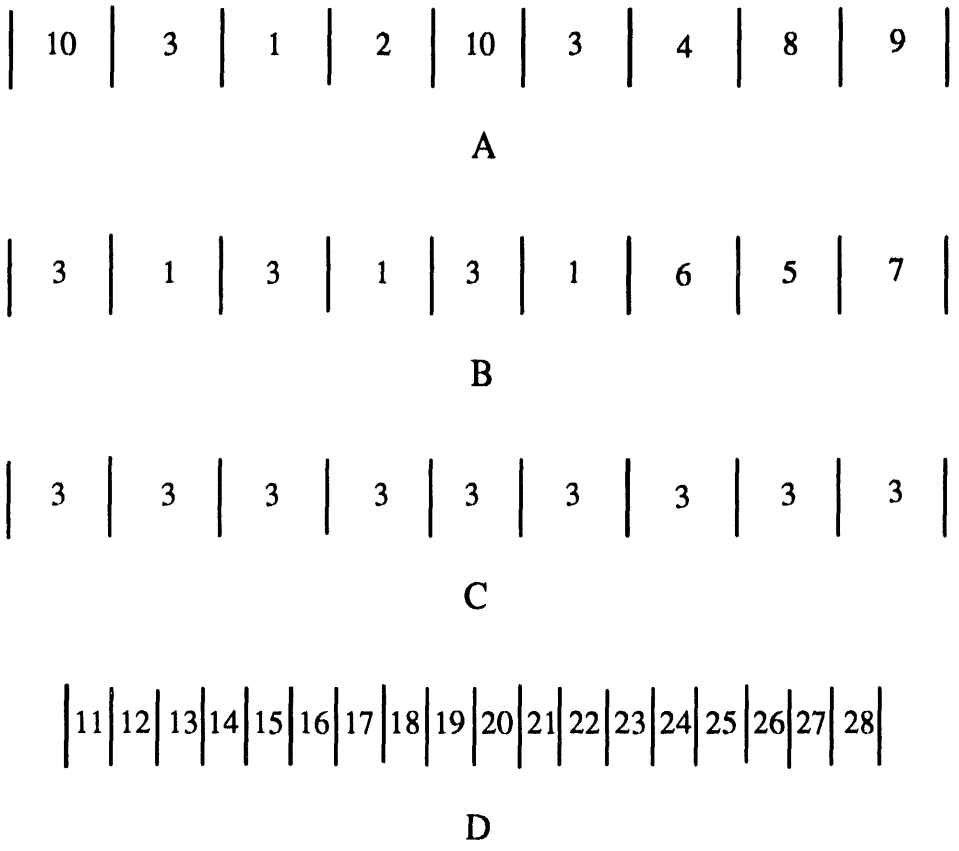

Figure 4.4 Salem - 1 models. A and B: all regions are 21.6 cm wide except the first region which is 10.8 cm wide,symmetry boundary conditions on the left, regions 7, 8, and 9 are reflectors. C: all regions are 20 cm wide, symmetry boundary conditions on the left. D: all regions are 20 cm wide.

Table 4.3 Macroscopic cross sections for Salem - 1.

Composition	Group	D_g (cm)	$\nu\Sigma_{fg}$ (cm^{-1})	Σ_g (cm^{-1})	$\Sigma_{gg'}$ (cm^{-1})
1	1	1.3648	0.005550	0.026132	0.017245
	2	0.4826	0.185823	0.130772	
2	1	1.3596	0.006267	0.025355	0.015398
	2	0.4798	0.230258	0.181915	
3	1	1.3592	0.006269	0.025232	0.015128
	2	0.4810	0.230923	0.188426	
4	1	1.3594	0.006890	0.025895	0.016386
	2	0.4673	0.264760	0.169073	
5	1	1.35890	0.006890	0.025711	0.015981
	2	0.46875	0.265512	0.177654	
6	1	1.3572	0.006894	0.025151	0.014752
	2	0.4740	0.268552	0.206951	
7	1	1.4957	0.0	0.025606	0.022923
	2	0.3637	0.0	0.051595	
8	1	1.3933	0.0	0.021484	0.017943
	2	0.3659	0.0	0.068149	
9	1	1.6701	0.0	0.032628	0.031408
	2	0.3621	0.0	0.039330	
10, 20-28	1	1.321964	0.005567	0.028660	0.015178
	2	0.486196	0.194976	0.211003	
11-19	1	1.321964	0.005567	0.028660	0.015178
	2	0.486196	0.194976	0.101003	

Table 4.4 Comparison of the node-average flux value for each node of Salem - 1. The value from Fourfour.f is larger by the percentage given.

A

Node	Group 1	Group 2	Node	Group 1	Group 2
1	5.3%	5.3%	19	-3.4%	-3.6%
2	5.3%	5.3%	20	-7.5%	-7.5%
3	5.3%	5.3%	21	-10.5%	-10.6%
4	5.3%	5.3%	22	-12.4%	-12.4%
5	5.3%	5.3%	23	-13.8%	-13.8%
6	5.4%	5.4%	24	-14.6%	-14.6%
7	5.4%	5.4%	25	-14.9%	-14.9%
8	5.7%	5.8%	26	-15.3%	-15.3%
9	6.4%	6.4%	27	-16.0%	-16.0%
10	6.6%	6.6%	28	-16.6%	-16.5%
11	6.5%	6.5%	29	-16.0%	-15.9%
12	6.2%	6.2%	30	-14.5%	-14.7%
13	5.3%	5.4%	31	-13.0%	-13.4%
14	4.6%	4.6%	32	-11.7%	-11.8%
15	4.1%	4.1%	33	-10.1%	-10.2%
16	3.4%	3.5%	34	-8.0%	-8.6%
17	2.3%	2.3%	35	-6.1%	-7.0%
18	0.1%	0.1%	36	-3.8%	-5.4%
Eigenvalue difference 0.03%					

B

Node	Group 1	Group 2	Node	Group 1	Group 2
1	3.5%	3.5%	10	-1.1%	-1.0%
2	3.8%	3.9%	11	0.2%	0.1%
3	5.3%	5.3%	12	-1.1%	-1.1%
4	5.2%	5.2%	13	-5.9%	-5.7%
5	2.6%	2.7%	14	-9.4%	-9.4%
6	2.1%	2.2%	15	-11.7%	-11.8%
7	3.9%	3.9%	16	-15.1%	-15.0%
8	3.3%	3.4%	17	-12.5%	-11.9%
9	0.1%	2.3%	18	2.6%	-0.4%
Eigenvalue difference 0.03%					

C

Node	Group 1	Group 2	Node	Group 1	Group 2
1	-0.013%	-0.012%	6	0.007%	0.007%
2	-0.012%	-0.012%	7	0.021%	0.021%
3	-0.010%	-0.010%	8	0.054%	0.054%
4	-0.006%	-0.006%	9	0.070%	0.071%
5	-0.001	-0.001%			
Eigenvalue difference 0.001%					

D

Node	Group 1	Group 2	Node	Group 1	Group 2
1	4.7%	4.7%	10	-5.9%	-6.0%
2	5.2%	5.1%	11	30.3%	31.2%
3	4.3%	4.3%	12	60.2%	59.3%
4	3.5%	3.5%	13	75.0%	75.4%
5	2.4%	2.5%	14	85.2%	85.1%
6	0.1%	0.1%	15	90.9%	91.0%
7	-0.1%	-0.1%	16	94.6%	94.5%
8	-0.6%	-0.6%	17	96.7%	96.7%
9	-3.0%	-2.9%	18	98.0%	98.0%
Eigenvalue difference 0.005%					

Table 4.4 gives the percent difference in the node-average fluxes for the two approximate models (second-order flux shape approximation in energy group one combined with a fourth-order approximation in energy group two and a fourth-order approximation in both energy groups). The nodes are numbered from left to right across the model shown in Fig. 4.4. Node sizes of 2.7 cm in the first four nodes of model A and 5.4 cm in rest of model A (four nodes per region), 5.4 cm in the first two nodes of model B and 10.8 cm in the rest of model B (two nodes per region), 20 cm in model C (one node per region), and 20 cm in model D (one node per region) were used to obtain the results given. These node sizes were used because it was determined that Fourfour.f gave accurate results for Salem - 1 for the respective node spacing in each model.

Table 4.4 shows that the eigenvalue from the unmixed approximation for model A is 0.03% larger than the eigenvalue from the mixed approximation (second-order flux shape

approximation in energy group one and a fourth-order approximation in energy group two). This fact suggests that the use of the mixed approximation for this problem is advantageous (results in little accuracy loss).

The difference in the node-average fluxes from the two approximate models for model A ranges from -16.6% to 6.6% in energy group one and -16.5% to 6.6% in energy group two with most of the values greater than 5% in absolute value. The largest difference, in absolute value, for both energy groups of model A occurs in node 28. This node corresponds to the region just before the reflector regions (See Fig. 4.4). However, this region is not the only fueled region that has differences of greater than 10%. These facts suggest that the use of the mixed approximation for model A with four nodes per region is not advantageous. Increasing the number of nodes per region may change this result but it will also increase the computing time (adding a disadvantage to the mixed approximation).

Based on the differences in the node-average fluxes from both energy groups and the eigenvalue difference, the use of the mixed approximation when applied to model A of Salem - 1 with four nodes per region is not advantageous.

Table 4.5 gives the percent difference in the node-average fluxes from a fourth-order approximation in both energy groups and a second-order approximation in both energy groups for model A. A comparison of the values in Table 4.5 (with absolute values ranging from 0.1% to 19.6% in energy group one and from 0.2% to 17.6% in energy group two) with those in Table 4.4 (with absolute values ranging from 0.1% to 16.6% in energy group one and from 0.1% to 16.5% in energy group two) shows that a second-order approximation in both energy groups does a better job at simulating the node-average fluxes than the mixed approximation for model A except in nodes 32 through 36 which correspond to the reflector.

Table 4.5 Comparison of the node-average flux value from a fourth-order approximation in both energy groups and a second-order approximation in both energy groups for each node of Salem - 1 model A. The value from the fourth-order approximation is larger by the percentage given.

Node	Group 1	Group 2	Node	Group 1	Group 2
1	-3.3%	-3.2%	19	2.2%	2.5%
2	-3.3%	-3.2%	20	4.4%	4.5%
3	-3.3%	-3.1%	21	5.9%	5.7%
4	-3.4%	-3.0%	22	7.0%	6.9%
5	-3.4%	-3.5%	23	7.7%	8.1%
6	-3.4%	-3.6%	24	8.2%	8.7%
7	-3.5%	-2.2%	25	8.7%	8.3%
8	-3.5%	-2.3%	26	9.1%	8.8%
9	-3.4%	-4.6%	27	9.3%	10.1%
10	-3.3%	-3.8%	28	9.4%	11.0%
11	-3.2%	-3.8%	29	10.1%	6.9%
12	-3.2%	-4.4%	30	11.3%	7.4%
13	-3.3%	-2.2%	31	12.4%	12.1%
14	-3.2%	-2.1%	32	13.4%	14.7%
15	-3.1%	-3.0%	33	14.6%	12.8%
16	-2.8%	-3.9%	34	16.2%	12.3%
17	-1.9%	-1.0%	35	17.8%	15.3%
18	-0.1%	0.2%	36	19.6%	17.6%
Eigenvalue difference -0.03%					

Figure 4.5 shows a plot of the flux for model A as a function of position in each energy group for the two approximate models. The position increases from left to right across model A shown in Fig. 4.4. The node boundaries are designated by the vertical lines one each plot. Figure 4.5 shows that the flux from the two approximate models is substantially different in nodes 9 through 13 and 19 through 28 for energy group one and nodes 25 through 29 for energy group two.

Figure 4.5
Energy Group One Flux as a Function of Position for Salem - 1 Model A

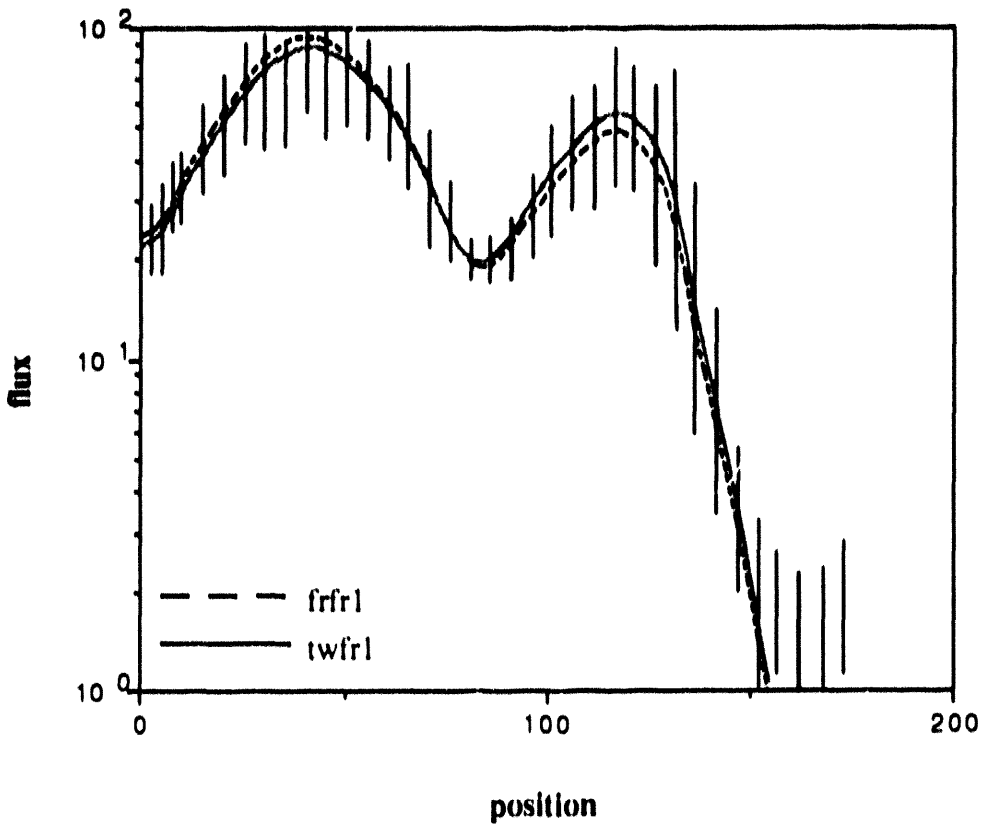

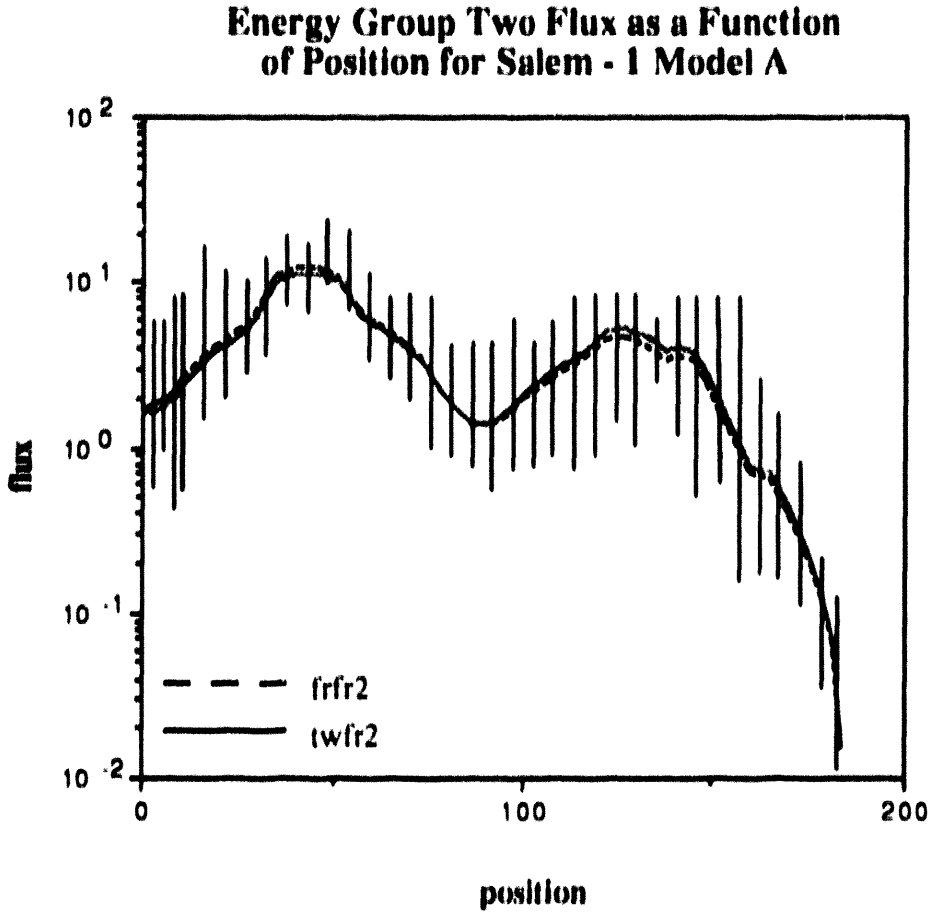

Table 4.4 shows that the eigenvalue from the unmixed approximation for model B is 0.03% larger than the eigenvalue from the mixed approximation (second-order flux shape approximation in energy group one and a fourth-order approximation in energy group two). This fact suggests that the use of the mixed approximation for this problem is advantageous (results in little accuracy loss).

The difference in the node-average fluxes from the two approximate models for model B ranges from -15.1% to 5.3% in energy group one and -15.0% to 5.3% in energy group two. The largest difference, in absolute value, for both energy groups of model B occurs in node 16 which corresponds to the region just before the reflector region, region 5 (See Fig. 4.4). This region and the reflector region are the only two that have difference values

greater than 10% in absolute value. However, there are two additional regions that have differences of greater than 5%, in absolute value, for both energy groups. These facts, suggest that the use of the mixed approximation for model B with two nodes per region is borderline advantageous.

Based on the differences in the node-average fluxes from both energy groups and the eigenvalue difference, the use of the mixed approximation when applied to model B of Salem - 1 with two nodes per region is borderline advantageous.

Table 4.6 Comparison of the node-average flux value from a fourth-order approximation in both energy groups and a second-order approximation in both energy groups for each node of Salem - 1 model B. The value from the fourth-order approximation is larger by the percentage given.

Node	Group 1	Group 2	Node	Group 1	Group 2
1	-1.4%	-0.6%	10	0.004%	2.2%
2	-1.6%	0.9%	11	0.7%	-1.3%
3	-1.3%	-2.7%	12	1.1%	-1.0%
4	-1.3%	-3.3%	13	1.5%	3.8%
5	-1.4%	0.8%	14	2.4%	3.7%
6	-1.2%	1.0%	15	3.3%	3.0%
7	-0.9%	-2.8%	16	3.6%	6.9%
8	-0.7%	-2.6%	17	6.8%	-1.5%
9	-0.5%	1.7%	18	19.3%	1.1%
Eigenvalue difference -0.08%					

Table 4.6 gives the percent difference in the node-average fluxes from a fourth-order approximation in both energy groups and a second-order approximation in both energy groups for model B. A comparison of the values in Table 4.6 (with absolute values ranging from 0.004% to 19.3% in energy group one and from 0.6% to 6.9% in energy group two) with those in Table 4.4 (with absolute values ranging from 0.1% to 15.1% in energy group one and from 0.1% to 15.0% in energy group two) shows that a second-order approximation in both energy groups does a better job at simulating the node-average fluxes than the mixed approximation for model B except in node 18 which corresponds to the reflector.

Figure 4.6
Energy Group One Flux as a Function of Position for Salem - 1 Model B

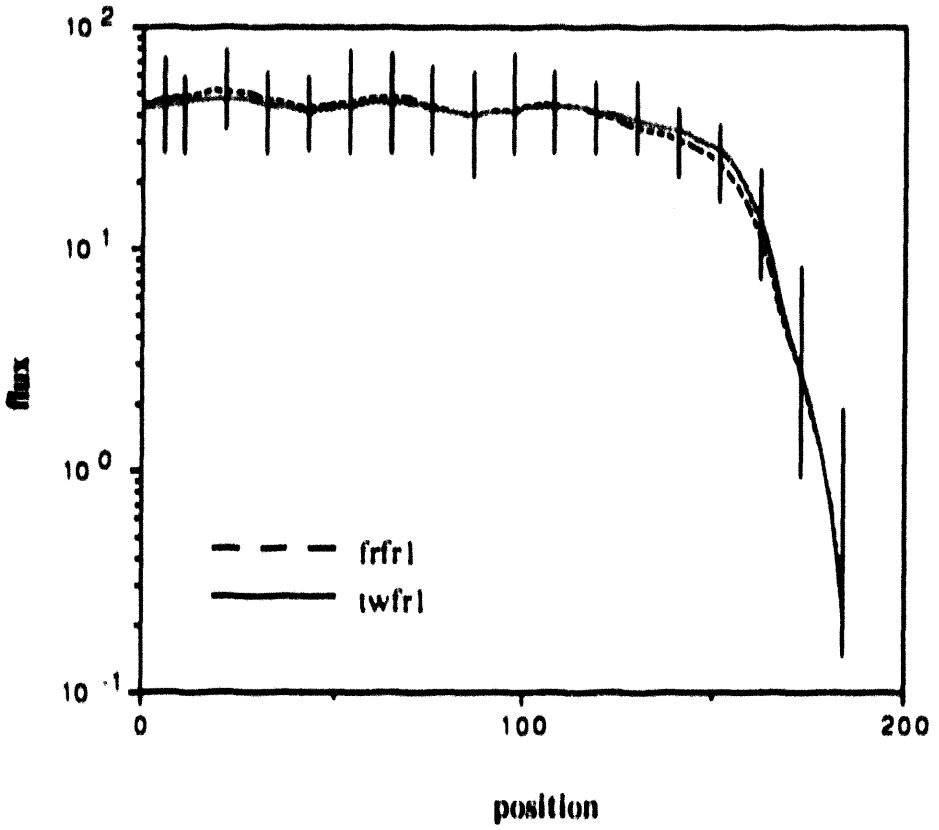

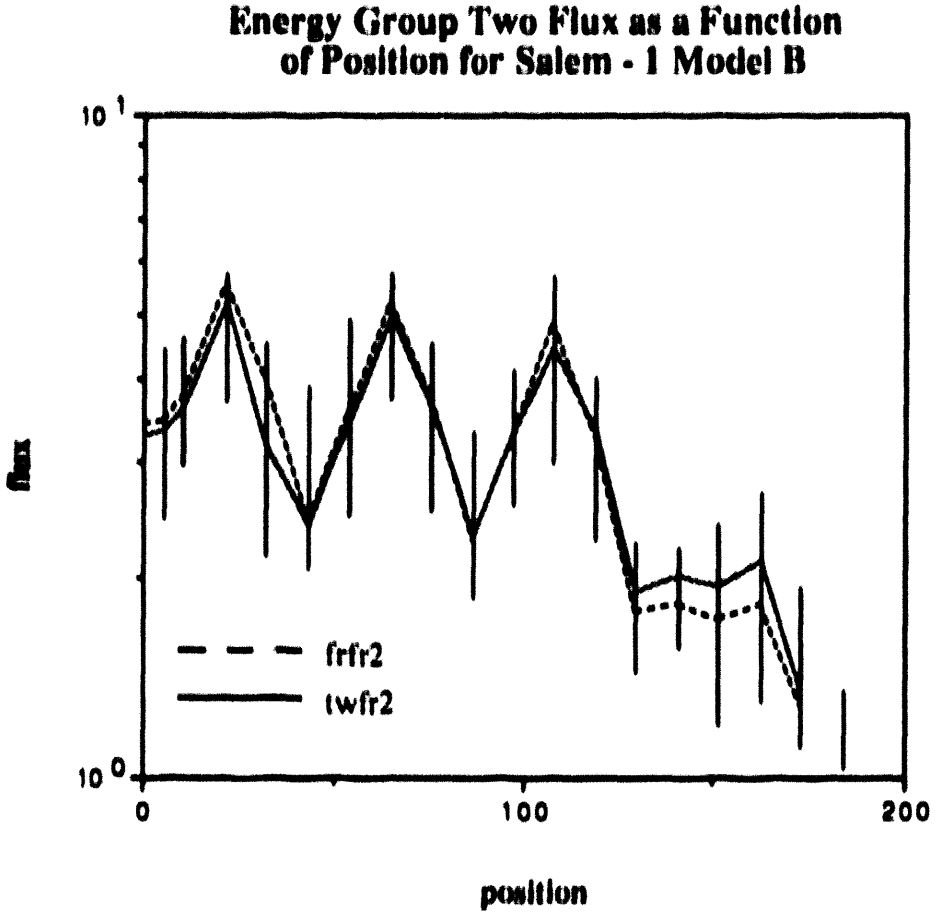

Figure 4.6 shows a plot of the flux for model B as a function of position in each energy group for the two approximate models. The position increases from left to right across the model shown in Fig. 4.4. The node boundaries are designated by the vertical lines on each plot. Figure 4.6 shows that the flux from the two approximate models is substantially different in nodes 3, 4, 14, 15, and 16 for energy group one and 4, 5, 14, 15, 16, and 17 for energy group two. Note that the plot for energy group two has an unrealistic shape. This shape is probably due to the method used to obtain the flux as a function of position. However, the shape should be investigated before making any conclusions for model B.

Table 4.4 shows that the eigenvalue from the unmixed approximation for model C is 0.001% larger than the eigenvalue from the mixed approximation (second-order flux shape approximation in energy group one and a fourth-order approximation in energy group

two). This fact suggests that the use of the mixed approximation for this problem is advantageous (results in little accuracy loss).

The difference in the node-average fluxes from the two approximate models for model C ranges from -0.013% to 0.070% in energy group one and -0.012% to 0.071% in energy group two. The values in both energy groups again suggest that the use of the mixed approximation for this problem is advantageous.

Based on the differences in the node-average fluxes from both energy groups and the eigenvalue difference, the use of the mixed approximation when applied to model C of Salem - 1 is advantageous.

Figure 4.7

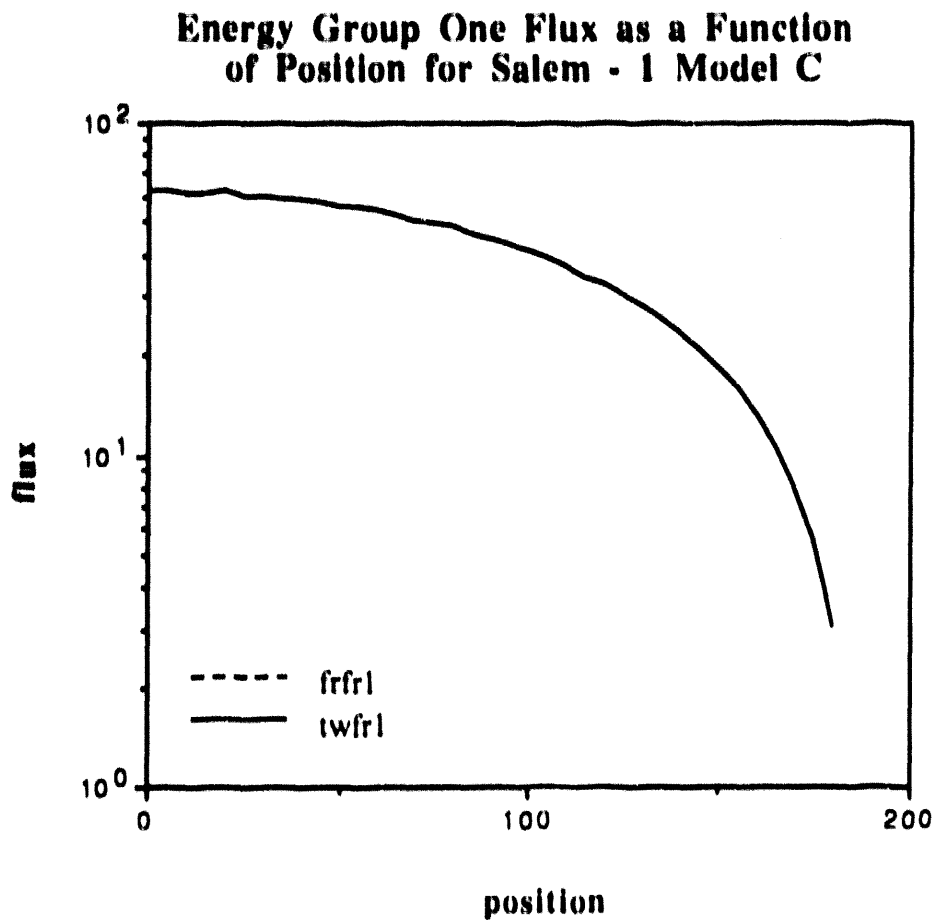

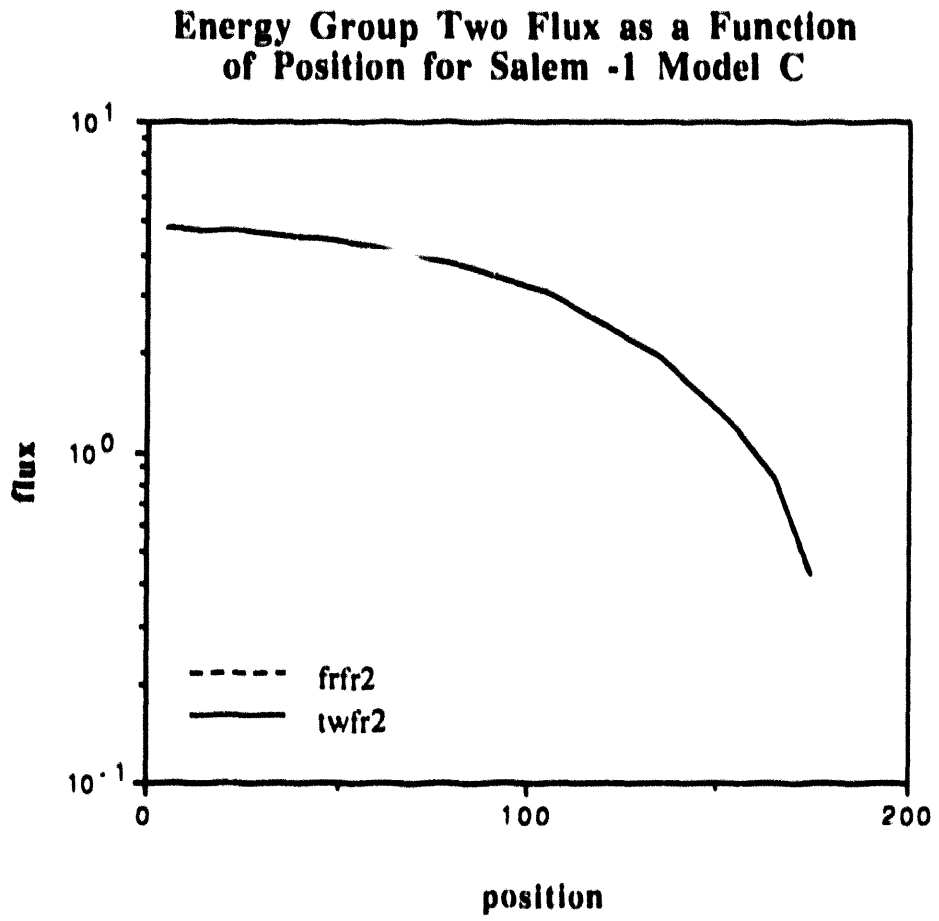

Figure 4.7 shows a plot of the flux for model C as a function of position in each energy group for the two approximate models. The position increases from left to right across model C shown in Fig. 4.4. The plot for energy group one in Fig. 4.7 shows that the flux from the two approximate models is essentially the same. This is also the case for energy group two. The flux from the two approximate models is essentially the same in Fig. 4.7 for energy group two.

Table 4.4 shows that the eigenvalue from the unmixed approximation for model D is 0.005% larger than the eigenvalue from the mixed approximation (second-order flux shape approximation in energy group one and a fourth-order approximation in energy group

two). This fact suggests that the use of the mixed approximation for this problem is advantageous (results in little accuracy loss).

The difference in the node-average fluxes from the two approximate models for model D ranges from -5.9% to 98.0% in energy group one and -6.0% to 98.0% in energy group two. The large difference values in both energy groups in nodes 11 through 18 suggest that the use of the mixed approximation for this problem is not advantageous. However, increasing the number of nodes per region, model D uses one node per region, may change this result but it will also increase the computing time (adding a disadvantage to the mixed approximation).

Figure 4.8

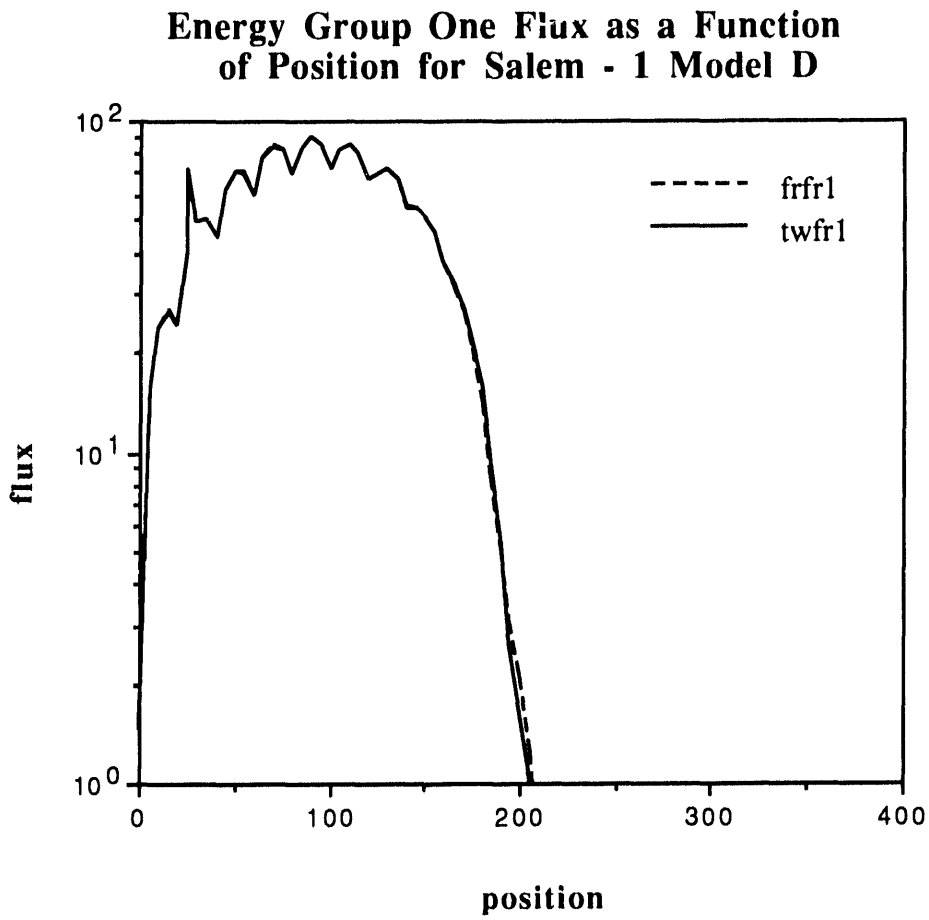

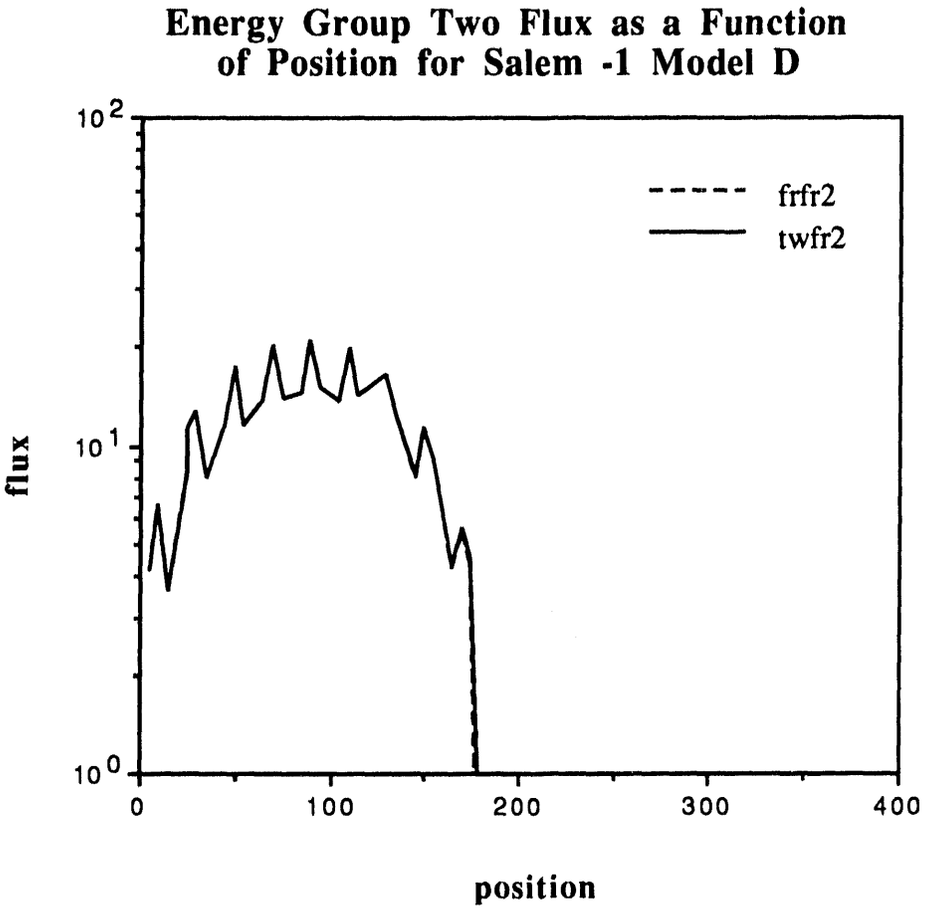

Based on the differences in the node-average fluxes from both energy groups and the eigenvalue difference, the use of the mixed approximation when applied to model D of Salem - 1 with one node per region is not advantageous.

Figure 4.8 shows a plot of the flux for model D as a function of position in each energy group for the two approximate models. The position increases from left to right across model D shown in Fig. 4.4. The plot for energy group one in Fig. 4.8 shows that the flux from the two approximate models is essentially the same. This is also the case for energy group two. The flux from the two approximate models is essentially the same in Fig. 4.8 for energy group two. Note that the plot has an unrealistic shape for both energy groups.

The shape is probably due to the method used to obtain the flux as a function of position. However, the shape should be investigated before making any conclusions for model D.

The second test problem used for LWRs was the 3D IAEA Benchmark Problem (see Section 4.3). Figure 4.9 shows the order of the compositions in the one-dimensional slice used. The macroscopic cross sections corresponding to the compositions in Fig. 4.9 are given in Table 4.7.

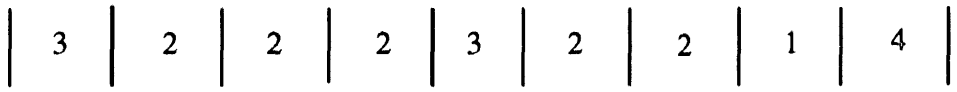

Figure 4.9 IAEA reactor model. All regions are 20 cm except the first region which is 10 cm wide. symmetry broundary conditions on the left. Region 4 is a reflector.

Table 4.7 Macroscopic cross sections for IAEA Benchmark.

Composition	Group	D_g (cm)	$\nu\Sigma_{fg}$ (cm^{-1})	Σ_g (cm^{-1})	$\Sigma_{gg'}$ (cm^{-1})
1	1	1.5	0.0	0.03	0.02
	2	0.4	0.135	0.08	
2	1	1.5	0.0	0.03	0.02
	2	0.4	0.135	0.085	
3	1	1.5	0.0	0.03	0.02
	2	0.4	0.135	0.13	
4	1	2.0	0.0	0.04	0.04
	2	0.3	0.0	0.01	

Table 4.8 Comparison of the node-average flux value for each node of the IAEA Benchmark.The value from Fourfour.f is larger by the percentage given.

Node	Group 1	Group 2	Node	Group 1	Group 2
1	33.0%	33.0%	10	-1.6%	-1.7%
2	33.0%	33.0%	11	-5.7%	-5.8%
3	33.4%	33.4%	12	-8.2%	-8.2%
4	32.9%	32.9%	13	-11.2%	-11.2%
5	31.6%	31.6%	14	-14.6%	-14.7%
6	29.7%	29.7%	15	-19.3%	-19.2%
7	26.9%	26.8%	16	-20.8%	-18.8%
8	21.5%	21.7%	17	-10.8%	-9.7%
9	10.3%	10.6%	18	4.8%	-2.6%
Eigenvalue difference -0.6%					

Table 4.8 gives the percent difference in the node-average fluxes for the two approximate models (second-order flux shape approximation in energy group one combined with a fourth-order approximation in energy group two and a fourth-order approximation in both energy groups). The nodes are numbered from left to right across the model shown in Fig. 4.9. Node sizes of 5 cm in the first two nodes and 10 cm in rest of the nodes (two nodes per region) were used to obtain the results given. These node sizes were used because it was determined that Fourfour.f gave accurate results for the IAEA Benchmark for this node spacing.

Table 4.8 shows that the eigenvalue from the unmixed approximation is 0.6% smaller than the eigenvalue from the mixed approximation (second-order flux shape approximation in energy group one and a fourth-order approximation in energy group two). This fact

suggests that the use of the mixed approximation for this problem is advantageous (results in little accuracy loss).

The difference in the node-average fluxes from the two approximate models ranges from -20.8% to 33.4% in energy group one and -19.2% to 33.4% in energy group two. The large values in both energy groups for all nodes except nodes 10, 11, and 18 suggest that the use of the mixed approximation for this problem is not advantageous. This is reinforced by the fact that the largest difference values occur in the first nodes, those corresponding to the center of the core, not in the nodes near or in the reflector. However, increasing the number of nodes per region, this problem uses two nodes per region, may change this result but it will also increase the computing time (adding a disadvantage to the mixed approximation).

Based on the differences in the node-average fluxes from both energy groups and the eigenvalue difference, the use of the mixed approximation when applied to the IAEA Benchmark with two nodes per region is not advantageous.

Table 4.9 gives the percent difference in the node-average fluxes from a fourth-order approximation in both energy groups and a second-order approximation in both energy groups. A comparison of the values in Table 4.9 (with absolute values ranging from 1.1% to 33.6% in energy group one and from 1.0% to 26.9% in energy group two) with those in Table 4.8 (with absolute values ranging from 1.6% to 33.4% in energy group one and from 1.7% to 33.4% in energy group two) shows that a second-order approximation in both energy groups does a better job at simulating the node-average fluxes than the mixed approximation except in the reflector, nodes 17 and 18.

Table 4.9 Comparison of the node-average flux value from a fourth-order approximation in both energy groups and a second-order approximation in both energy groups for each node of the IAEA Benchmark. The value from the fourth-order approximation is larger by the percentage given.

Node	Group 1	Group 2	Node	Group 1	Group 2
1	-26.9%	-25.7%	10	-1.1%	1.0%
2	-27.1%	-24.9%	11	3.2%	2.1%
3	-26.1%	-26.9%	12	5.9%	5.7%
4	-24.8%	-25.2%	13	7.9%	8.0%
5	-23.6%	-23.6%	14	9.8%	9.7%
6	-22.0%	-21.9%	15	11.8%	13.9%
7	-19.9%	-20.1%	16	14.7%	19.4%
8	-16.4%	-18.1%	17	22.8%	12.1%
9	-9.1%	-7.0%	18	33.6%	10.8%
Eigenvalue difference 0.25%					

Figure 4.10 shows a plot of the flux as a function of position in each energy group for the two approximate models. The position increases from left to right across the model shown in Fig. 4.9. The node boundaries are designated by the vertical lines on each plot. Figure 4.10 shows that the flux from the two approximate models is substantially different in all of the nodes except nodes 10, 11, 12, 17, and 18 for energy group one. The flux from the models is also substantially different in all of the nodes for energy group two except nodes 10, 11, and 18.

Figure 4.10

Energy Group One Flux as a Function of Position for the IAEA Benchmark

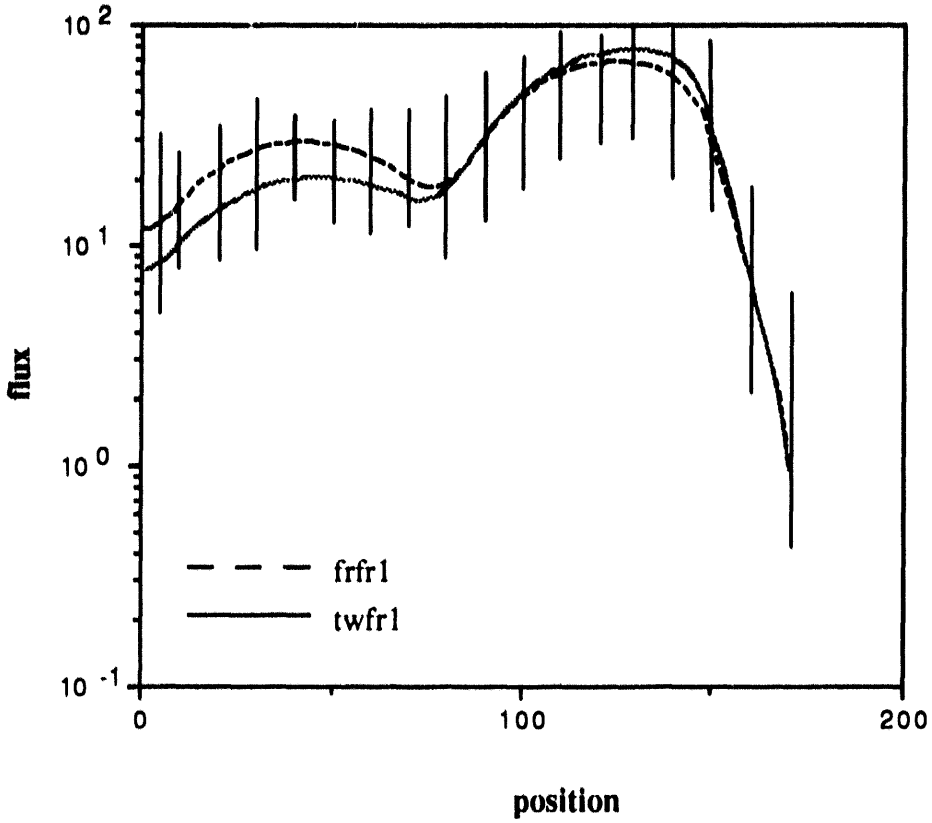

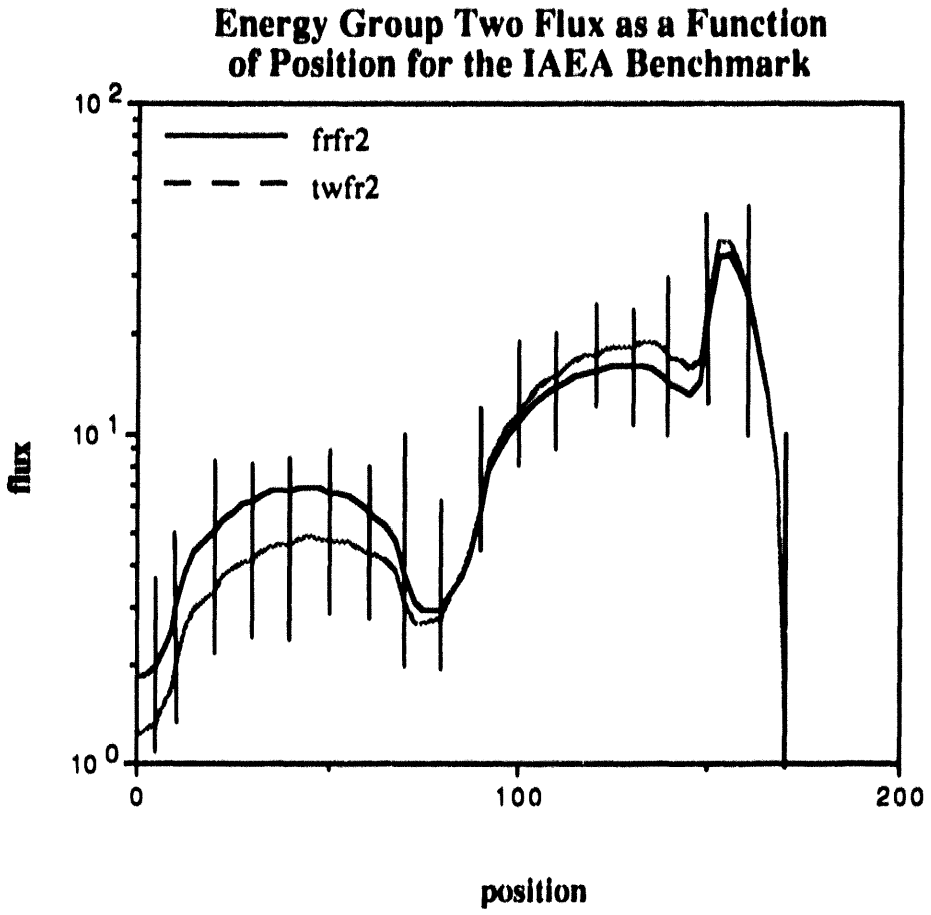

4.4.3 Heavy Water Reactor

The test problem used to model a heavy water reactor was a slice of a D_2O production reactor simulation. The one-dimensional slices used contain each of the four regions: reflector, target, control, and fuel, that make up the core. Figure 4.11 shows the order of the four regions in the two slices used. The macroscopic cross sections corresponding to each region in Fig. 4.11 are given in Table 4.10. The boundary conditions used are zero returning current at the core external edges and no net current at the center of the core.

A

B

Figure 4.11 Production reactor simulation model. All regions are 18 cm wide. A has symmetry boundary conditions on the right.

Table 4.10 Macroscopic cross section for production reactor.

Region	Group	D_g (cm)	$\nu\Sigma_{fg}$ (cm^{-1})	Σ_g (cm^{-1})	$\Sigma_{gg'}$ (cm^{-1})
fuel	1	1.38504	2.85416×10^{-3}	8.86506×10^{-3}	6.44203×10^{-3}
	2	0.898526	3.70310×10^{-2}	2.18825×10^{-2}	
target	1	1.17097	1.50390×10^{-3}	1.29105×10^{-2}	7.67664×10^{-3}
	2	0.880244	8.81440×10^{-3}	1.36547×10^{-2}	
control	1	1.31919	0.0	1.20594×10^{-2}	1.16912×10^{-2}
	2	0.901342	0.0	5.63097×10^{-3}	
reflector	1	1.29000	0.0	8.02913×10^{-3}	8.00000×10^{-3}
	2	0.883000	0.0	7.96268×10^{-3}	

Table 4.11 Comparison of the node-average flux value for each node of the production reactor simulation.The values from Fourfour.f are larger by the percentage given.

A

Node	Group 1	Group 2	Node	Group 1	Group 2
1	9.2%	6.0%	6	5.3%	3.1%
2	7.8%	5.5%	7	4.2%	2.4%
3	6.5%	4.9%	8	1.0%	1.2%
4	5.1%	4.2%	9	-0.5%	0.1%
5	4.5%	3.7%	10	-0.8%	-0.5%
Eigenvalue difference -0.77%					

B

Node	Group 1	Group 2	Node	Group 1	Group 2
1	9.0%	6.2%	11	-0.04%	0.6%
2	7.5%	5.5%	12	2.5%	1.9%
3	5.8%	4.5%	13	4.2%	2.5%
4	4.1%	3.8%	14	1.7%	1.6%
5	3.7%	3.4%	15	-0.7%	2.7%
6	4.8%	3.0%	16	-1.5%	-0.7%
7	4.2%	2.3%	17	-0.8%	-0.4%
8	0.9%	1.1%	18	0.9%	0.4%
9	-0.8%	0.02%	19	2.7%	1.4%
10	-1.0%	-0.3%	20	4.3%	2.1%
Eigenvalue difference -0.65%					

Table 4.11 gives the percent difference in the node-average fluxes for the two approximate models (second-order flux shape approximation in energy group one combined with a fourth-order approximation in energy group two and a fourth-order approximation in both energy groups). The nodes are numbered from left to right across the model shown in Fig. 4.11. Node sizes of 9 cm were used to obtain the results given. These node sizes were used because it was determined that Fourfour.f gave accurate results for model A and model B of the production reactor simulation for this node spacing.

Table 4.11 shows that the eigenvalue from the unmixed approximation for model A is 0.77% smaller than the eigenvalue from the mixed approximation (second-order flux shape approximation in energy group one and a fourth-order approximation in energy group two). This fact suggests that the use of the mixed approximation for this problem is advantageous (results in little accuracy loss).

The difference in the node-average fluxes from the two approximate models for model A ranges from -0.8% to 9.2% in energy group one and -0.5% to 6.0% in energy group two. The largest difference values for both energy groups occur in the first two nodes, corresponding to the reflector region (See Fig. 4.11). Therefore, the values in both energy groups again suggest that the use of the mixed approximation for this problem is advantageous.

Based on the differences in the node-average fluxes from both energy groups and the eigenvalue difference, the use of the mixed approximation when applied to model A of the production reactor simulation is advantageous.

Figure 4.12 shows a plot of the flux for model A as a function of position in each energy group for the two approximate models. The position increases from left to right across model A shown in Fig. 4.11. The plot for energy group one shows that the flux from the two approximate models is essentially the same. This is also the case for energy group two. The flux from the two approximate models is essentially the same in Fig. 4.12 for energy group two.

Figure 4.12

Energy Group One Flux as a Function of Position for the Production Reactor Simulation Model A

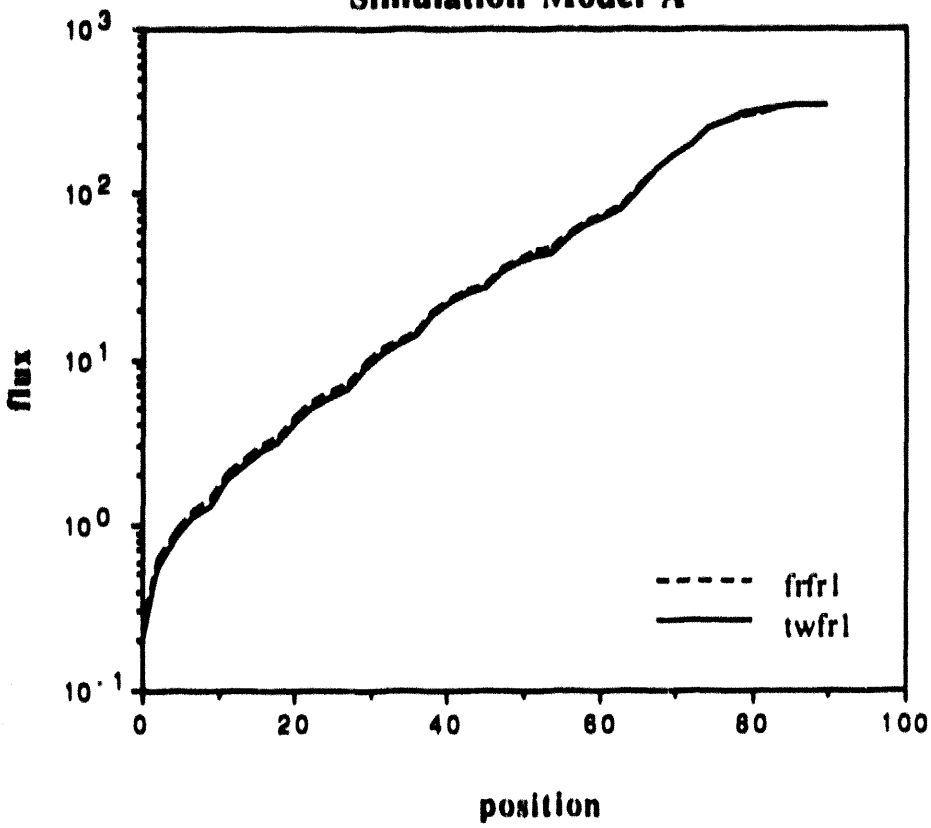

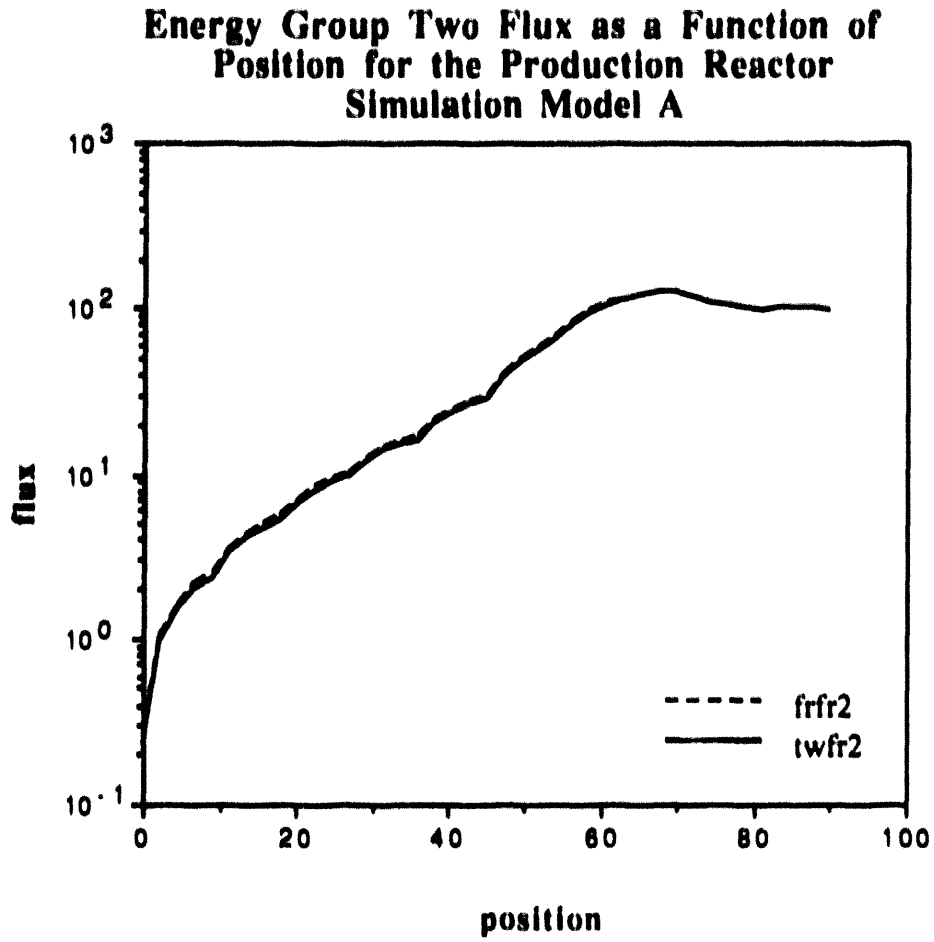

Table 4.11 shows that the eigenvalue from the unmixed approximation for model B is 0.65% smaller than the eigenvalue from the mixed approximation (second-order flux shape approximation in energy group one and a fourth-order approximation in energy group two). This fact suggests that the use of the mixed approximation for this problem is advantageous (results in little accuracy loss).

The difference in the node-average fluxes from the two approximate models for model B ranges from -1.5% to 9.0% in energy group one and -0.7% to 6.2% in energy group two. The largest difference values for both energy groups occur in the first few nodes, corresponding to the reflector region (See Fig. 4.11). The difference values in the remaining nodes for both energy groups are all less than 5%. Therefore, the values in both

energy groups again suggest that the use of the mixed approximation for this problem is advantageous.

Based on the differences in the node-average fluxes from both energy groups and the eigenvalue difference, the use of the mixed approximation when applied to model B of the production reactor simulation is advantageous.

Figure 4.13
Energy Group One Flux as a Function of Position for the Production Reactor Simulation Model B

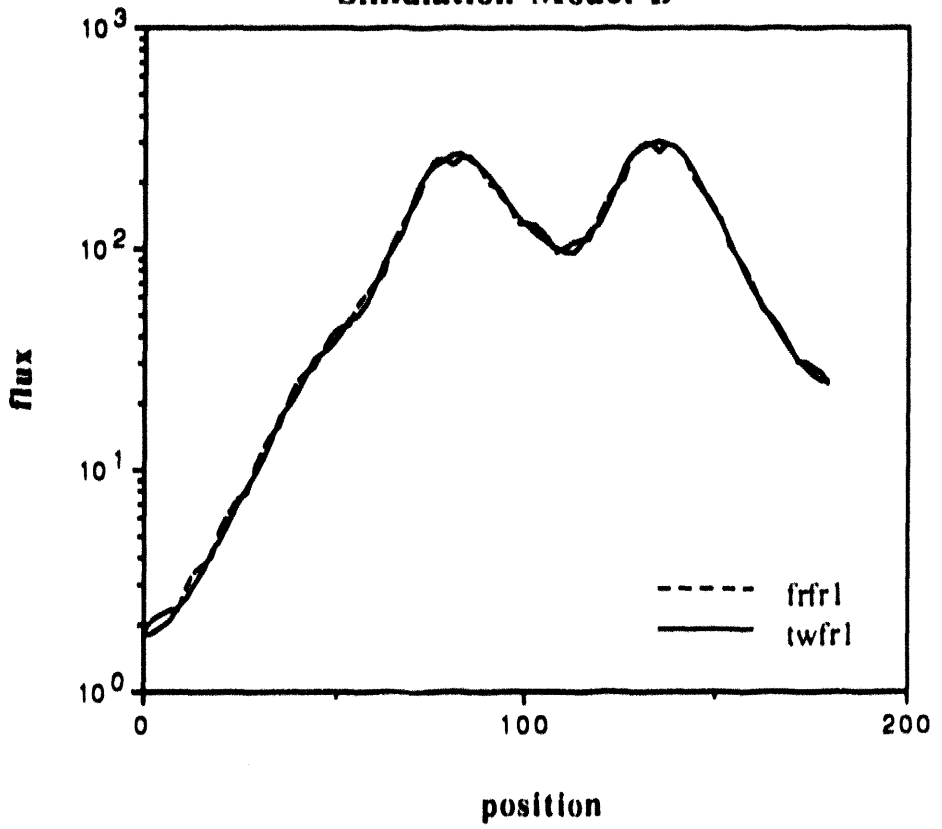

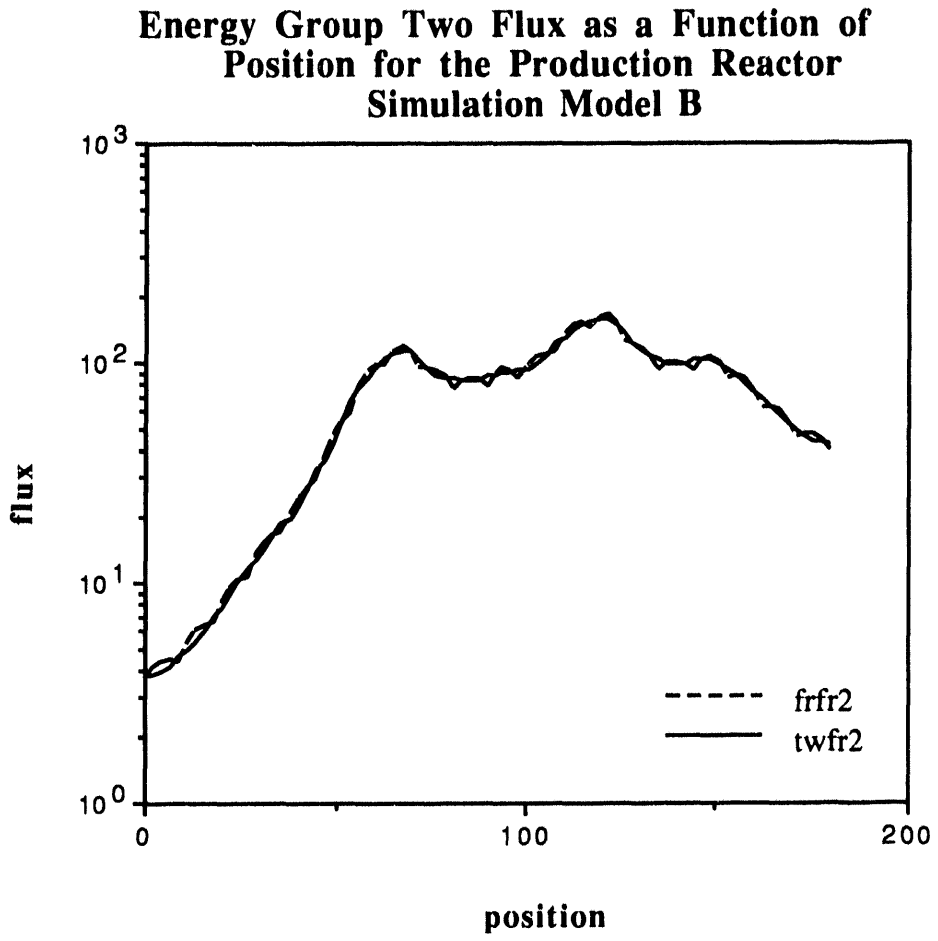

Figure 4.13 shows a plot of the flux for model B as a function of position in each energy group for the two approximate models. The position increases from left to right across model B shown in Fig. 4.11. The plot for energy group one shows that the flux from the two approximate models is essentially the same. This is also the case for energy group two. The flux from the two approximate models is essentially the same in Fig. 4.13 for energy group two.

4.5 Summary

The application of the solution method has been presented in this chapter. Three reactor types were modeled to examine the usefulness of the quadratic flux shape approximation in energy group one and quartic flux shape in energy group two. Because the solution method presented in Chapter 3 involves coupled equations and two iteration loops, computer programs were written to aid the solution. The results from the two computer programs for graphite reactor, pressurized water reactor, and heavy water reactor test problems were presented.

Chapter 5 discusses the conclusions that can be drawn from the results presented in this chapter. Also included in Chapter 5 are some recommendations for further study relating to the use of mixed flux shape approximations.

Chapter 5

CONCLUSIONS AND RECOMMENDATIONS

5.1 Conclusions

The use of a second-order flux shape approximation in energy group one and a fourth-order flux shape approximation in energy group two (the mixed approximation) as compared to a fourth-order flux shape approximation in both energy groups results in considerable loss in accuracy. The accuracy loss, in node-average flux, occurs for pressurized water reactors composed of homogeneous regions of varying compositions. This accuracy loss is probably due to the inability of the mixed approximation to account for the changes in the flux shape across the core. Because the accuracy loss is large for the pressurized water reactor modeled, the mixed approximation should not be used for this type of reactor composed of homogeneous regions of varying composition.

The mixed approximation does not result in large losses in accuracy for the heavy water reactor and the graphite reactor modeled . This is the case since a quadratic function is probably sufficient to simulate the flux in energy group one for these two reactor types. The mixed approximation can be used for heavy water and graphite reactors.

The overall conclusion from the present numerical comparisons is that further investigation into the accuracy and computing time is necessary before any quantitative advantage of the use of the mixed approximation can be determined.

5.2 Recommendations

The work performed in this thesis considered slices of reactors composed of homogeneous regions. One area to investigate is the inclusion of heterogeneities in the regions. A good way to include these heterogeneities is to use discontinuity factors. If the discontinuity factors are found for groups of regions using a second-order flux shape

approximation in energy group one and a fourth-order flux shape approximation in energy group two then the factors could account for the shape approximation as well as the heterogeneity. With the discontinuity factors accounting for both items, the results obtained could be better than the results obtained in this thesis.

Another area to investigate in order to examine the benefits of using a mixed approximation is the computing time for each approximation. The computer programs associated with this thesis were written to test accuracy not computational speed. However, it is a combination of speed and accuracy that is needed when solving for the neutron flux across the reactor core.

References

1. S. Glasstone and A. Sesonske, Nuclear Reactor Engineering, Van Nostrand Reinhold Company, Inc., New York, 1981.

2. A. F. Henry, Nuclear-Reactor Analysis, The M.I.T. Press, Cambridge, M.A., 1975.

3. J.C. Gehin, "A Nodal Method for the Solution of the Static, Few-Group, Diffusion Equations in Hexagonal Geometry," SM Thesis, Department of Nuclear Engineering, M.I.T., (February 1990).

4. M. H. Kim, "The Use of Bilinearly Weighted Cross Sections for Few-Group Transient Analysis," PhD Thesis, Department of Nuclear Engineering, M.I.T., (June 1988).

5. J. C. Gehin, personal communication, 1991.

DATE FILMED

1/10/94

END